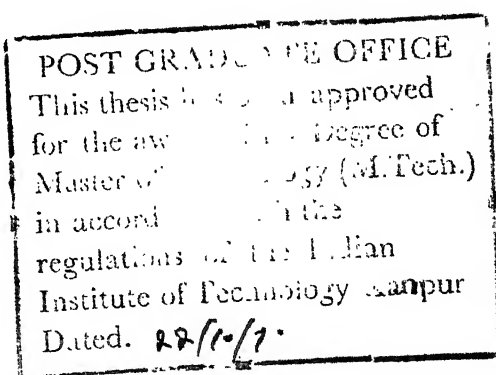


# A Study of The Oxidation Behaviour of Zirconium-2.5 Weight Percent Niobium Alloy

A Thesis Submitted  
In Partial Fulfilment of the Requirements  
For the Degree of  
Master of Technology

By  
HARISH CHANDRA SINGH



to the

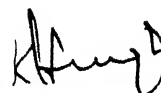
DEPARTMENT OF METALLURGICAL ENGINEERING  
INDIAN INSTITUTE OF TECHNOLOGY KANPUR

OCTOBER, 1970

609.735  
S664  
A 432

# CERTIFICATE

Certified that this work on 'A Study of the Oxidation Behaviour of Zirconium - 2.5 wt. pct. Niobium Alloy' has been carried out under my supervision and that it has not been submitted elsewhere for a degree.



(K.P. Singh)  
Associate Professor  
Dept. of Metallurgical Engineering  
Indian Institute of Technology Kanpur

ME-1970-M-SIN-STV

POST GRADUATE OFFICE
This thesis has been approved
for the award of the degree of
Master of Technology (M.Tech.)
in accordance with the
regulations of the Indian
Institute of Technology Kanpur
Dated.

## ACKNOWLEDGEMENTS

This work was carried out under the supervision of Dr. K.P. Singh whose continuing encouragement and many valuable suggestions must be most gratefully acknowledged.

Thanks are due to Dr. A.S. Parasnis for his assistance during taking photomicrographs with polarizing-microscope, to Dr. R.N. Patil for his help in making a differential thermal analysis.

I would also like to extend my sincere thanks to Mr. A. Jayaraman of Thermodynamics Laboratory, Mr. K.P. Mukherjee of Physical Metallurgy Laboratory, Mr. K.N.S. Rao of Physics Research Laboratory, Mr. N. Ram of X-ray Laboratory, Mr. D. Madhavarao of Engineering Geology Laboratory and Mr. M. Rehman of Materials Testing Laboratory for their assistance in various measurements.

My appreciations towards the facilities extended by Central Workshop, Glass Blowing Section, Central Instrumentation Laboratory and 7044 Computer Machine are duly recorded. In the last, I thank Mr. J.K. Misra for his careful and efficient typing of this thesis.

H. C. Singh

## CONTENTS

CHAPTER		Page
	SYNOPSIS	ix
1.	INTRODUCTION	1
2.	EXPERIMENTAL	15
	2.1 Specimen Preparation	15
	2.2 Weight-gain Measurements	17
	2.3 Examination of the Oxidation Products	22
3.	THERMOGRAVIMETRY	26
	3.1 Reproducibility of the Results	35
	3.2 Effect of Thermal Cycling	36
	3.3 Effect of Temperature and Time	40
	3.4 Mechanism of Oxidation	49
	3.5 Effect of Medium of Oxidation	53
	3.6 Effect of History of the Samples	57
	3.7 Activation Energies	57
4.	PHYSICAL FEATURES OF OXIDE FILMS, AND METALLOGRAPHY	61
	4.1 Physical Features	61
	4.2 Macrographs	65
	4.3 Micrographs	69



CHAPTER		Page
	4.3.1 Micrographs with Ordinary Light	69
	4.3.2 Micrographs with Polarized Light	74
5.	POWDER PATTERNS, AND DIFFERENTIAL THERMAL ANALYSIS	76
	5.1 Powder Patterns	76
	5.2 Differential Thermal Analysis	82
6.	DIFFRACTOGRAMS	85
7.	MICROHARDNESS	89
8.	GENERAL DISCUSSIONS	94
9.	NEED OF FUTURE WORK	100
APPENDIX A	Zr-Nb System	104
	Zr-O System	105
APPENDIX B	ASTM - data for X-ray Analysis	106
	REFERENCES	108

## LIST OF FIGURES

FIGURE		Page
1.	Reaction Chamber and Weight Recording Units	19
2.	Gas Train	21
3.	Weight-gain Curves (linear-plot, Category I)	37
4.	Weight-gain Curves (linear-plot, Category II)	38
5.	Weight-gain Curves (linear-plot, Category III)	39
6.	Weight-gain Curves (double log-plot, Category I)	44
7.	Weight-gain Curves (single log-plot, Category I)	45
8.	Weight-gain Curves (double log-plot, Category II)	46
9.	Weight-gain Curves (double log-plot, Category III)	47
10.	Arrhenius Plot	58
11.	Temperature Thermogram of an Alloy Powder Sample	83
12.	A Part of the Diffractogram Taken with Sample V	87
Appendix A	Zirconium - Niobium System	104
	Zirconium - Oxygen System	105

## LIST OF TABLES

TABLE	Page
1. Classification of the Samples	16
2. Basic Informations about the Samples	26
3. Thermogravimetric Data	28
4. Variation of n and k in equation $w^n = kt$	41
5. Comparison of Initial Kinetics for Oxidation in Air and in Oxygen	55
6. Physical Features of the Oxidized Samples	61
7. Calculated d-Values from Powder Patterns	77
8. Identified Oxidation Products from the Powder Patterns	81
9. Diffractogram - readings for Sample Seven	85
10. Knoop Hardness for the Unoxidized Specimens	90
11. Knoop Hardness for the Oxidized Specimens	91
Appendix B ASTM - data for X-ray Analysis	106

## LIST OF PICTURES

	Page
Macrographs ( $M_1 - M_4$ )	66
Macrographs ( $M_5 - M_9$ )	67
Micrographs ( $M_{10} - M_{20}$ )	70
Micrographs ( $M_{21} - M_{27}$ )	71
Micrographs ( $M_{28} - M_{35}$ )	72
Micrographs ( $M_{36} - M_{38}$ )	75

## SYNOPSIS

The oxidation behaviour of Zr - 2.5 weight percent Nb alloy varied depending on (1) temperature of oxidation (2) elapsed time of oxidation (3) medium of oxidation, and (4) history of the specimens.

Rate of oxidation increased, as expected, with increase in temperature. At low temperatures ( $300^{\circ}\text{C}$  or so) the kinetics could possibly be described by logarithmic law whereas at elevated temperatures parabolic and linear rate laws were observed. At around  $700^{\circ}\text{C}$  and above the rate was far more enhanced.

Appreciable oxidation occurred only above  $350^{\circ}\text{C}$ . Above  $500^{\circ}\text{C}$ , the weight-gain was rapid, and at temperatures higher than about  $700^{\circ}\text{C}$  the rate was very high. This temperature dependence behaviour seemed to be reflected in the peaks observed during differential thermal analysis of the powder specimen.

With elapsed time of oxidation at a constant temperature, a number of transition cycles in the weight gain curves were observed. Explanation to this was sought in terms of characteristics of oxides of niobium formed during the reaction. Other processes which could explain the occurrence of transition have been separately considered. The explanations were supported by metallographic observations and X-ray analysis

of the substrate and the reaction products. Attempt to correlate the number of oxide layers observed under polarizing microscope with that of transition cycles failed due probably to the separate layers of oxide not being distinctly resolved with the magnification employed.

Oxidation in air was rapid compared to that in oxygen. The difference in the weight-gains for the two cases decreased with increasing temperature of oxidation. This has been explained on the basis of a mechanism based on diffusion model for growth of the oxide layer and increasing reactivity of niobium with nitrogen with increasing temperature evidenced from literature.

The oxidation of annealed samples led to slower rate compared to that for the case of as-received ones. This was amenable to theoretical explanation based on the coarseness of the second phase observed from the micrographs.

Results of hardness measurements and diffractograms led to a conclusion that oxygen penetration in the substrate at lower temperature (500°C or so) for extended oxidation, or for short duration at elevated temperatures as were the case in the present work, occurred to a very small depth. This has been correlated with activation energy for diffusion of oxygen in the metal.

Calculated activation energies for different kinetics observed were correlated with the possible processes occurring in the oxidation reaction.

Results of X-ray analysis, microhardness measurements, diffractograms, macrographs, micrographs and observed oxide layers under polarizing microscope have been discussed to correlate with the kinetics observed.

## CHAPTER 1

### INTRODUCTION

Until the late 1940's little was known about the corrosion resistance of zirconium, either because of the scarcity of the pure metal or variable purity of the metal available.

Zirconium and its alloys have been a subject of extensive study due to their growing importance in the field of nuclear technology and chemical industries. Their importance in nuclear reactor as structural materials mainly lies due to low neutron absorption cross-section, good mechanical strength and tolerable corrosion resistance.

The utility of zirconium and its alloys in nuclear reactor applications has stimulated much study of their corrosion behaviour. The mechanism and kinetics have been explored by a number of investigators<sup>1-4</sup> using such variants as temperature, pressure, alloy composition and time duration. However, their results are of conflicting nature. It is realized that even the mechanism of oxidation of commercially pure zirconium has not been clearly understood within



the entire range of many variables, let alone the case of the alloy of the metal.

Pure zirconium is soft and susceptible to high corrosion. The metal has therefore to be alloyed to put it to a suitable use as structural materials. Zircaloy-2, an alloy of zirconium, with Sn 1.5, Fe 0.12, Cr 0.10 and Ni 0.05 pct., has been widely acclaimed for its use in the nuclear reactors as cladding material for the fuel element. In the recent past, another alloy of zirconium containing 2.5 wt. pct. niobium seemed to hold more promise<sup>3</sup> to substitute zircaloy-2 in view of its slightly improved strength and corrosion resistance property over the latter.

Both of these alloys have been investigated for their behaviour mainly in water and steam because most of the reactors use these media for cooling and as moderator. Literature survey reveals that little work has been done to delineate their behaviour in gaseous environments other than steam (details of literature survey are given elsewhere). Hence it is desirable that the kinetic behaviour of the alloys in pure oxygen and air be well understood.

The Zr-2.5 wt. pct. Nb alloy, due to its unique properties, could possibly be used as structural materials for the future power reactors. The present investigation was carried out with a view to understand the behaviour of the

alloy both in air and pure oxygen at different temperatures under a pressure of one atmosphere. The runs were carried out thermogravimetrically and the reaction products analysed by different methods.

<sup>An</sup>  
All extensive literature survey on oxidation characteristics of pure zirconium, Niobium and their alloys was made and is summarised in the following few pages.

### Zirconium:

Little significant attack occurs during oxidation of zirconium with common gases below 400°C. Above this temperature, the metal reacts with oxygen, nitrogen and water vapour. The rate increases rapidly with increasing temperature.

Reaction of zirconium with oxygen was extensively studied by many workers in the past.<sup>5-13</sup> Gulbransen and Andrew<sup>5</sup> studied effect of temperature in the range 200-425°C and pressure 0.76 - 7.6 mm. Although no single rate law fitted their data,<sup>a</sup> they found that a modification of parabolic rate law predicts the general shape of the time-curve. Cubicciotti<sup>6</sup> studied oxidation in the range 600-950°C which includes the condition where oxygen is reacting with the metal and the oxide is dissolving in the metal phase. His results showed parabolic law at all temperatures except 920°C where small deviation towards linear relationship was observed. Calculated activation energy was 32.0 kcal./mole.

Latter investigators,<sup>14,15</sup> however maintained that their results are more adequately expressed by cubic equations.

Despite many conflicting results, the laws governing reaction of zirconium with oxygen may be summarised as follows. The oxidation is logarithmic below 300-400°C. Above 400°C, the reaction behaviour changes. It has been found that the value of  $n$  in the general rate equation  $w^n = kt$  varies from three<sup>12,14,16,17</sup> to two<sup>6,16,18</sup>. The reason for these divergencies is not clear. Gulbransen and Andrew,<sup>16</sup> and Pemsler<sup>19</sup> proposed that they may be related to the surface preparation of the specimens and differences in orientation between different grains.

In an electron microscope study of zirconium oxidation Douglass and van Landuyt<sup>20</sup> showed that the thin oxide films as viewed by transmission microscopy are extremely heterogeneous despite the fact that the films show uniform interference colours and exhibit smooth surfaces by the replication techniques. On this basis, these authors question the usefulness of expressing the kinetic measurements in terms of particular rate equations.

Holmberg et al.,<sup>21</sup> Gebhardt et.al.<sup>22</sup> and Domagla<sup>23</sup> found solid solubility of oxygen in  $\alpha$  - zirconium to be 29 atomic percent between 400 and 800°C (See Appendix A). The solubility

was independent of temperature. Oxygen occupies interstitial positions (octahedral) in the zirconium lattice. Introduction of oxygen beneath the metal surface results in hardening of it. It was suggested by Treco<sup>10</sup> that the extensive hardening effect must be due in part to the lattice distortion accompanying its introduction and possibly to the preferred position of the oxygen atoms.

Pemler<sup>24</sup>, Wallwork et al.,<sup>18</sup> and Westerman<sup>25</sup> showed that the oxygen dissolution process followed a parabolic rate above 600°C, and they also found that the solubility of oxygen in zirconium at 850°C was 60 at. pct. or less. The stable oxide of zirconium is  $ZrO_2$ . It exists in three crystallographic forms: cubic, tetragonal and monoclinic.

From their electron diffraction study of the oxide film formed on zirconium between 300 and 600°C, Hickman and Gulbransen<sup>26</sup> showed that the monoclinic form of  $ZrO_2$  was present. Most X-ray diffraction studies on oxide films formed below 1000°C revealed only the presence of monoclinic  $ZrO_2$ , while electron diffraction studies on thin films also indicated the formation of cubic (or tetragonal) modifications. The monoclinic form is thermodynamically stable below about 1200°C<sup>27</sup> whereas tetragonal modification is stable at higher temperatures. Douglass and Landuyt<sup>20</sup> also observed pseudo-amorphous regions in thin  $ZrO_2$  films.

It is generally agreed that  $\text{ZrO}_2$  may be oxygen-deficient, but the extent of non-stoichiometry of  $\text{ZrO}_2$  in equilibrium with oxygen-saturated zirconium is not known. As lower oxides of zirconium are non-existent, the maximum non-stoichiometry in monoclinic  $\text{ZrO}_2$  is probably small.

From marker studies it is concluded that oxygen ions migrate inward through the scale. It is also generally assumed that the defects in non-stoichiometric  $\text{ZrO}_2$  consist of oxygen vacancies. The exact nature of the defect structure of  $\text{ZrO}_2$ , the transport numbers of electrons, anions and cations are not known.

At 300-700°C, the thin dark grey or bluish-black scales formed by oxidation in oxygen are tightly adherent to the metal<sup>9,26</sup>. As the temperature is raised further white spots of  $\text{ZrO}_2$  and accompanying flakiness appear,<sup>9,28</sup> the spots increasing in size until almost the whole specimen is white (after 24h at 700°C, and a few minutes at 900°C). With oxidation in <sup>air</sup> above 1050°C the inner black scale, consisting of monoclinic and tetragonal  $\text{ZrO}_2$  and cubic  $\text{ZrH}$ , occupies most of the thickness.<sup>29</sup>

It is well known<sup>30,31</sup> that the reaction of nitrogen with zirconium is negligible at low pressure and temperature below 400°C. The reaction proceeds slowly at 400°C but quite appreciably<sup>5</sup> at 800°C or above.

Fast<sup>7</sup> found that nitrogen upto 20 at. pct. formed a solid solution with zirconium. Nitrogen atoms like those of oxygen, are absorbed in the interstices of the metal lattice but have less mobility. The dissolved nitrogen increases  $\alpha - \beta$  transition temperature in same way as does oxygen although to a greater extent. The reaction rate has been found to be parabolic<sup>5,32</sup> upto 1000°C. The rate was also independent of pressure. The activation energies were calculated to be 39.2 and 50 kcal./mole respectively.

The solid solubility limit of nitrogen in zirconium was found to be 20 at. pct. Cubic nitride  $ZrN$  is formed in addition to the saturated hexagonal solution. The nitride is golden yellow in colour.

A relatively higher scaling rate of zirconium in air as compared to that of zirconium in oxygen or nitrogen was reported by Phalnikar and Baldwin<sup>29</sup>. Belle and Mallet<sup>14</sup> showed that the kinetics of the high temperature oxidation of zirconium in air followed a cubic rate law. The activation energy for the reaction was calculated to be 47.2 kcal./mole. Kendall<sup>33</sup> studied the oxidation rates of zirconium in dry air at 500, 600 and 700°C. The rate initially followed a cubic rate and finally it became a linear one. The activation energy was calculated to be 41.4 kcal/mole for the initial reaction and 29.8 kcal/mole after transition to the linear rate.



Someno<sup>34</sup> determined reaction rates of pure zirconium with oxygen, nitrogen and air at high temperatures. The reactions mainly followed parabolic rate law. The activation energies for these reactions were: 34.2 kcal/mole, 35.0 kcal/mole and 42.2 kcal/mole for reaction in oxygen, nitrogen and air respectively.

After initial protective oxidation zirconium and zirconium-base alloys begin to oxidize at an accelerated rate. Much effort has been expended to unravel the reaction mechanism, but yet no clear-cut explanation has been offered and the reason for the increased rate of oxidation is still obscure.

#### Niobium:

The reactions between niobium and oxygen have been studied over a wide range of conditions, often with conflicting results. The temperature dependence of niobium - oxygen reaction may be viewed in three stages: between 200 and 375°C a protective oxide is formed, and the reaction follows a parabolic rate law; no transition to another mechanism has been observed.<sup>35</sup> Between 375° and about 500°C the reaction, although initially parabolic, becomes linear after a maximum period of 6 hours.<sup>36</sup> About 550°C, the reaction is essentially linear.

Hurlen et al.<sup>37</sup> proposed a general oxidation curve. They applied it to the reaction of niobium with oxygen for a wide range of temperatures and pressures. The curve involved at least five stages of oxidation (although all stages were not present at every temperature and pressure).

Below 500°C, and above 700°C the rate of oxidation increases, as might be expected, with increasing temperature.<sup>35,36</sup> Conflicting results have been reported for the oxidation behaviour of niobium with oxygen <sup>within</sup> between temperature range 500 – and 650°C.

According to Brauer<sup>38</sup>, niobium forms three oxides, viz., NbO, NbO<sub>2</sub> and Nb<sub>2</sub>O<sub>5</sub>. Hurlen<sup>39</sup> has suggested the existence of an additional oxide, Nb<sub>2</sub>O, but it is not confirmed. The oxide Nb<sub>2</sub>O<sub>5</sub> exists in different allotropic forms.

The reaction of niobium with nitrogen follows a simple parabolic rate law between 400 and 1600°C.<sup>40</sup>

Nb-N system is complex. Presence of small amount of carbon or oxygen can lead to the formation of a number of new phases. Schönberg<sup>41</sup> and recently Guard et al.<sup>42</sup> have reported that there exist five phases in Nb-N system. According to the latter, these phases are: (i)  $\alpha$  - NbN<sub>0.02</sub> (bcc), (ii)  $\beta$  - Nb<sub>2</sub>N (NbN<sub>0.40-0.52</sub>) - hcp, (iii)  $\gamma$  - Nb<sub>4</sub>N<sub>3</sub> (NbN<sub>0.75-0.8</sub> - fcc), (iv)  $\delta$  - NbN (NbN<sub>0.88-0.91</sub>) fcc and (v)  $\epsilon$  - NbN (NbN<sub>0.92-1.00</sub>) - hcp.



Albrecht and Goede<sup>43</sup> found, in their study of reaction of niobium with nitrogen, that an Arrhenius plot of parabolic rate constant showed a change in the reaction mechanism at 1000°C. Below this temperature, a mixture of Nb<sub>2</sub>N and NbN is produced, whereas the high temperature reaction produces only NbN.

Reaction with air shows that at low temperatures, the reaction is initially parabolic.<sup>40</sup> It becomes linear with the passage of time (21 hours at 400°C). Above 600°C, the reaction is linear almost from the start. A break in the temperature dependence of the niobium reaction rate curve was observed by Inouye<sup>44</sup> at around 880°C and was associated with the formation of Nb<sub>2</sub>O<sub>5</sub>. It was later questioned by Klopp et al.<sup>45</sup>.

The effect of moisture in air on reaction with niobium is open to question. It has been observed that increasing the humidity at 400-600°C increases the rate of oxidation.<sup>46</sup> However, it has also been reported that an increase in humidity at 600°C leads to a decrease in the rate of oxidation.<sup>44</sup> At temperatures higher than 800°C, moisture has no effect on the rate of oxidation.<sup>44</sup>

#### Zirconium-Niobium Alloys:

Cox<sup>47</sup> and Dalgaard<sup>48</sup> have studied the corrosion resistance behaviour of a range of Zr-Nb alloys both in water and

high pressure steam upto  $300^{\circ}\text{C}$ . Their study suggested that Zr-2.5 wt. pct. Nb alloy has corrosion resistance acceptable to power reactors<sup>48</sup>. Dalgaard suggested from study of the effect of heat treatment that the amount of niobium in a solid solution controls the rate of oxidation, and that concentration, size and distribution of a second phase is of little importance.

Cox et al.<sup>48</sup> showed that corrosion of Zr-Nb alloys with high percent (20 to 60 pct) niobium was susceptible to non-uniform oxidation and considered unsuitable for use as structural materials in water or steam.

Presence of  $\alpha$ ,  $\beta$  and  $\omega$  phases have been reported by many investigators.<sup>49,50</sup> Bethune and Williams<sup>49</sup> recently investigated by electron probe microanalysis ( $\alpha + \beta$ )/ $\alpha$  phase boundary (See Appendix A). Nb is observed to be soluble upto 1.1 wt. pct. in  $\alpha$  - Zr at  $600^{\circ}\text{C}$ . The  $\beta$ - $\alpha$  transformation has been found by Guerlet and Lehr<sup>51</sup> to be very sluggish in nature. Thus phase boundary compositions of Zr-Nb system given in Appendix A may be considered to be approximate.

Bryant<sup>52</sup> measured solubility of oxygen in Nb-Zr alloys. He found that the solubility of oxygen in transition alloys is largely electronic in nature. If e/a ratio of the alloy is greater than 5.75, the solubility is small; where as it is large in case of lower e/a ratio.

In oxidation of Zr-Nb alloys, an intermediate compound  $6 \text{ ZrO}_2 \cdot \text{Nb}_2\text{O}_5$  has often been observed<sup>51,53,54</sup> apart from the simple oxides of the metals. But this compound forms when the alloy contains high amount of Nb. Prokoshkin<sup>54</sup> thought that the rate of oxidation is strongly affected due to formation of this compound.

Greenbank and Harper<sup>55</sup> found, in <sup>their</sup> this investigation of solute distribution in oxidised Zr-Nb alloys by electron beam microanalysis, that Nb dissolves in the oxide  $\text{ZrO}_2$  with little alteration to the oxide structure.

Prokoshkin et al.<sup>54</sup> observed from their X-ray study that the solubility of  $\text{ZrO}_2$  in  $\beta\text{-Nb}_2\text{O}_5$  is of the order of 30 mole percent.

While the oxidation of Nb-base zirconium alloys has been shown<sup>56,57</sup> to exhibit internal oxidation, no such behaviour has been observed for the case of Zr-base alloys.

The oxide on specimen surface generally undergoes the changes in colour from black to mottled and finally to white. Black oxide is thought to be protective and non-stoichiometric whereas white is non-protective and stoichiometric. Dalgaard<sup>3</sup> thought that the effect of Nb in non-stoichiometric black oxide may be to increase the tolerance for oxygen - that is, to enable the oxide to be very close to stoichiometry without losing the characteristics of the black oxide.

Zmeskal et al.<sup>58</sup> measured rates of oxidation of 17 alloys of Zr and Nb metals by a volume procedure for periods of 2-6 hours. At 600°C, the oxidation of the alloys was approximately parabolic ( $w^2 = kt$ ) during the early stages of oxidation. At 900°C, the general relation  $w^n = kt$  was not followed by any of the alloys in the oxidation process, but all appeared to increase gradually in rate towards a linear relation. At 1090°C, value of  $n$  was observed to vary from about 3 for alloys low in Nb to 2 for alloys high in Nb. Oxidation of the alloys at 900°C, resulted in mixed oxides consisting of two or three phases: monoclinic  $ZrO_2$ , orthorhombic  $6 ZrO_2 \cdot Nb_2O_5$  and  $Nb_2O_5$  (low temperature form). A fourth phase, the high temperature form of  $Nb_2O_5$  was found in most of the oxides formed at 1090°C.

Perte et al.<sup>59</sup> made investigations to see the effects of 1-4 at percent of 20 elements on the oxygen uptake of zirconium at 700°C and  $pO_2 = 200$  mm. They concluded that the addition of Nb decreased the oxidation resistance and showed, in addition, a transition after a few minutes or hours to linear oxidation. This transition normally occurs with pure zirconium at a much higher temperature, accompanying a deterioration in the adherence of the scale.

In a study of Nb(base) - Zr alloys, Hiltz<sup>60</sup> took X-ray diffraction patterns on the scale and on the interface between metal and the scale. <sup>He</sup> They observed presence of  $\text{Nb}_2\text{O}_5$ . In addition to this oxide, <sup>he</sup> they observed a second set of  $d$ -spacings which could not be identified with the lines of any known oxides of the elements. The diffraction pattern from the metal/scale interface showed lines for  $\text{NbO}$  and  $\text{Nb}$ . It was interpreted that  $\text{Nb}_2\text{O}_5$  provides little protection and rate is controlled by  $\text{NbO}$ . The mechanism by which  $\text{NbO}$  controlled the rate was not clear.

In their investigation of oxidation of zirconium-niobium alloys (1-20 pct. Nb) in  $\text{CO}_2$  gas at 750 and 900°C, Guerlet and Lehr<sup>51</sup> observed that oxidation was rapid at 750°C and slower at 900°C. They ascribed this behaviour to the nature of oxidation products. The oxide surface at 750°C showed fissures on it. With increasing temperature, the tendency of formation of a complex oxide  $6 \text{ZrO}_2 \cdot \text{Nb}_2\text{O}_5$  was thought to increase.

## CHAPTER 2

### EXPERIMENTAL

#### Materials:

Reactor grade Zr - 2.5 wt. pct. Nb alloy was obtained from Bhabha Atomic Research Centre, Bombay and was used in the present investigations.

#### Gases:

Cylinder oxygen (commercial grade) was dried by passing over sulphuric acid solution, dry calcium chloride and finally over ascarite. Air was dried by a similar method. Oxygen gas used was 99.7 pct. pure.

#### 2.1 Specimen Preparation:

Specimens were made by cutting as received alloy ingots with jewel saw. Thirty four rectangular samples were made in total which varied in thickness and surface area (see Table 2).

The specimens were divided into three categories on the basis of their subsequent oxidation and heat treatment as given in Table 1. Categories I, II and III consisted of eight, fifteen and eleven specimens in number respectively. As mentioned in Table 1, the samples in category III were annealed at 800°C for one hour at a pressure of  $10^{-6}$  mm.

Table 1  
Classification of Samples

Category I	Category II	Category III
1. as received	1. as received	1. annealed at 800°C for 1 hr. under 10-6 mm pressure of mercury.
2a. oxidized for long duration of time (upto 2245 mts.)	2a. oxidized for small period of time (5 - 240 mts.)	2a. oxidized for small period of time (10-410 mts.)
2b. oxidized at low temperatures (276 - 670°C)	2b. oxidized at high temperatures (554 - 869°C)	2b. oxidized at high temperatures (595-843°C)
3. designated in Roman numerals (from I to VIII)	3. designated in Arabic numerals (from 1 to 15)	3. designated in words (from one to eleven)

Polishing of the samples was done by the usual mechanical procedure employed in metal polishing. Polishing of the samples in categories I and II was done upto 4/0 emery paper. The samples in category III were polished upto the velvet cloth in which suspension of alumina particles was used abrasive.

The polished samples were etched by swabbing them for a proper time into a solution consisting of 45 pct. lactic acid, 45 pct. nitric acid and 10 pct. hydrofluoric acid. This etchant revealed the grain boundary clearly and etched the Nb-rich phase distinct. Use of glycerine in place of lactic acid did not produce satisfactory results. After etching, the



traces of etchant were removed by washing the samples under running tap water for more than half an hour. The samples were subsequently washed with alcohol.

## 2.2 Weight - Gain Measurements:

Schematic diagrams for the experimental set up and gas train are given in Fig. 1 and 2 respectively.

The recording semi-micro balance (manufactured by Wm. Ainsworth and Sons Inc, Colorado, USA) had an electronic indicating and recording device. It gave a continuous record of the weight changes occurring in the sample as a function of time on a graph paper. The balance had a sensitivity of 0.1 mg (i.e. of 4 chart division of 1/10 inch), readability by estimation of 0.01 mg and reproducibility of  $\pm 0.03$  mg. The span on the chart read 10 mg. Means to expand the recording range have been built into the recording balance. Whenever the recorder pen approached a chart edge, a weight of exactly one full-scale value was applied or removed to rescale the instrument. Enough weights for forty full-span steps have been provided. The capacity of the balance, viz., 100 gm was considerably larger than the recording range. The zero stability was fairly good.

The recording balance was used to record weight -gains for the samples. The sample under investigation was suspended from the hook beneath the left pan of the balance. Care was



always taken to keep the sample in the predetermined uniform temperature zone. It may be noted that the samples in category I were directly suspended through platinum wire hook. For that purpose a hole was drilled in the sample. However, a quartz crucible was employed for holding the samples in categories II and III which, in turn, was supported on a platinum loop to which the platinum wire connecting the pan was hooked. The furnace consisted of the winding of a 22-gauge nichrome wire upon a  $3\frac{1}{2}$  cm. sillimanite refractory tube. The overall resistance of the winding was around 50 ohms. The temperature in the uniform zone of the furnace was controlled within  $\pm 2^{\circ}\text{C}$  with the help of a temperature controller as shown in Fig. 1. The reaction tube made of quartz was connected to the balance through a brass flange with O-rings. In order to protect the balance from heat of the furnace, the flange was cooled by circulating water through copper tube.

A calibrated Chromel - Alumel thermocouple was used to record the temperature of the furnace. The junction of the thermocouple was kept as close as possible to the specimen in order to record its temperature as accurate as possible.

In all the runs, system was evacuated to a pressure below  $10^{-3}$  mm. with the help of a mechanical pump before it was filled with the oxidizing medium at one atmosphere. The vacuum was measured with the help of a thermocouple gauge. Pressures in milli-metre range upto one atm. and slightly

# LEGEND

1. balance chamber
2. gas inlet
3. water cooling
4. quartz tube
5. platinum wire
6. sillimanite tube
8. nichrome winding embedded in alundum cement
9. specimen
10. furnace shell
11. asbestos powder
12. weight recorder
13. temperature controller
- R. resistance
- T<sub>1</sub>. thermocouple to 13
- T<sub>2</sub>. thermocouple to external potentiometer

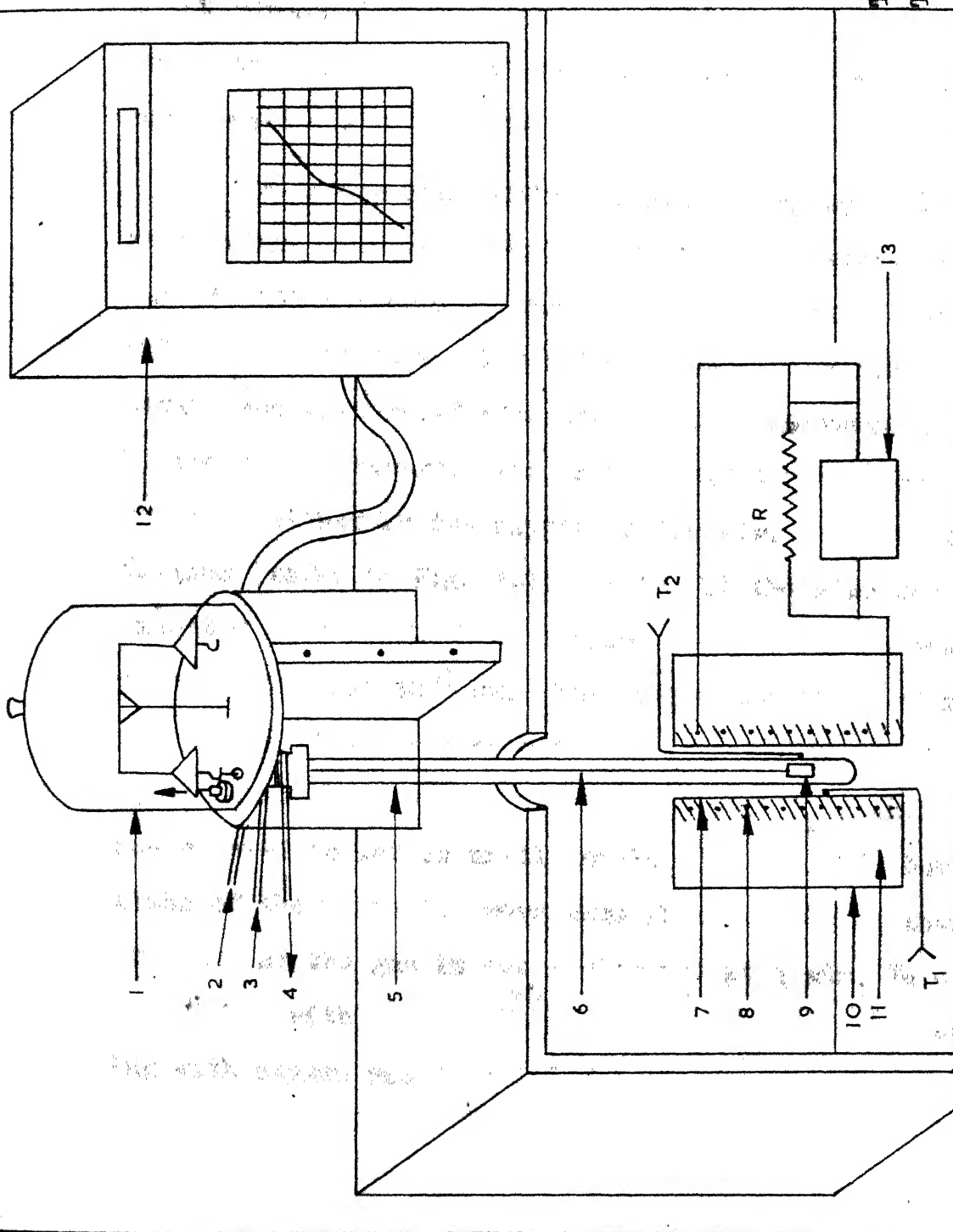
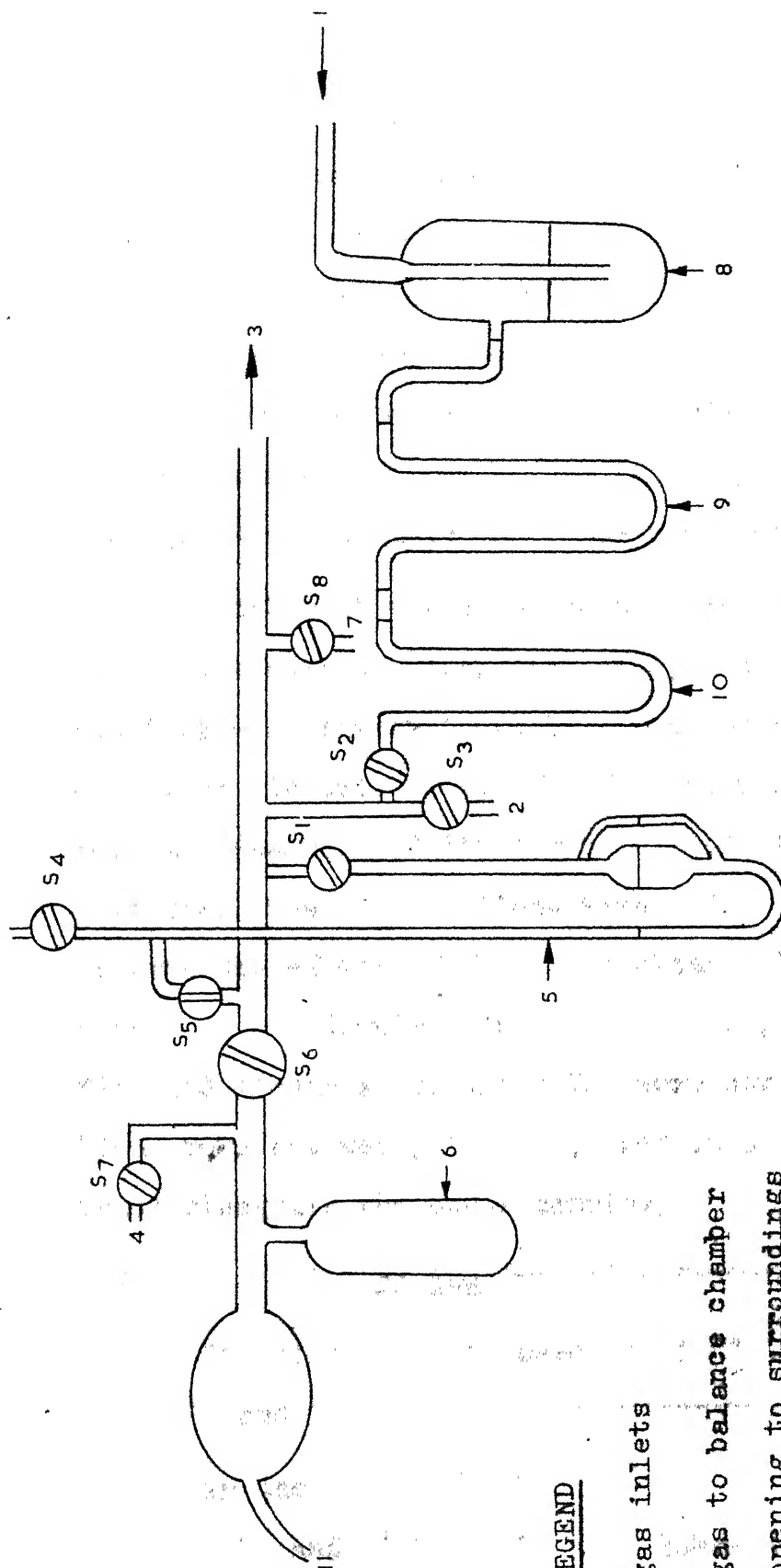


Fig. 1

above were measured with the help of a built-in mercury manometer (Fig. 2).

Before entering the reaction chamber, the gas was dried by allowing it to pass through gas-train consisting of dehydrant chambers numbered 8, 9 and 10 (Fig. 2) which contained sulphuric acid solution, dry calcium chloride and ascarite respectively.

Oxidation runs either in air or oxygen at a specified temperature were made after evacuating the system and refilling it with the desired gas. The run was taken according to following procedure. The balance was tested for its sensitivity and calibrated according to the instruction supplied by the manufacturers. Air in the reaction chamber was replaced either by dry oxygen or dry air. This was done as follows (refer to Fig. 1-2). With all the stop cocks closed, except  $S_5$  and  $S_6$  which were open, the system was evacuated to approximately  $10^{-3}$  mm. The system was detached from the pump by closing the stop cock  $S_6$ . The gas then entered the system through inlet 1 with the stop cock  $S_2$  open. The gas was allowed to let in until levels of mercury in both the limbs of the manometer were same thus indicating that the pressure of the gas in the system was at 1 atm. In case of runs taken with oxygen, <sup>the</sup> this process of evacuation and refilling with oxygen was repeated for three times in order to reduce



# **LEGEND**

- 1. gas inlets
- 2. gas to balance chamber
- 3. gas to balance chamber
- 4. opening to surroundings
- 5. manometer
- 6. liquid nitrogen trap
- 7. vacuum gauge contact
- 8. gas drying system
- 9. gas drying system
- 10. vacuum pump contact
- 11. vacuum pump contact

*Fig. 2*

GAS TRAIN (Schematic)

the impurities. After this, the furnace already maintained at specified temperature was raised with the help of a screw jack to a zone of the furnace in order to keep the sample in uniform temperature. Uniform temperature zone within the furnace extended over seven centimeters in length. The beam was then released and the recorder put on after the furnace containing the sample was set at proper position. The subsequent weight-gain curve was recorded on the chart.

Isothermal measurements were recorded during the runs. One of the samples, viz., Sample 2, was deliberately interrupted thrice at intervals to be mentioned elsewhere during the course of its oxidation. The furnace was removed from the reaction chamber and the sample allowed to cool to room temperature. The interruptions with this sample were made to observe the effect of thermal cycling. It may be mentioned here that the Sample 3 in a category II, and the Samples one, five and eleven in category III were not subjected to oxidation runs but were, however, used in other types of measurements alongwith the other samples.

### 2.3 Examination of the Oxidation Products:

Reaction products were examined by Metallography, X-ray analysis and Microhardness measurements.

In the metallographic technique, pictures showing macrographs and micrographs were taken with the help of optical microscope. The micrographs were taken at a magnification of

400. The pictures showed specimen surfaces before and after oxidation runs. Macrographs showed total specimen surface whereas the micrographs were taken to delineate metallurgical structures on the following locations of the samples: oxide surface, bare alloy substrate after descaling a part of the oxidized specimen, junction of the oxide/bare substrate surface, and interior and edges of the samples.

As mentioned above, a part of the oxidized specimen surface was descaled. The stripping was done with the help of a diamond file of 300 grit.

Pictures were taken on the stripped substrate after polishing and etching the surface by usual procedure mentioned earlier. The polishing was done upto velvet cloth.

To detect the oxide layers, a set of micrographs were taken through the cross section of the samples in polarised light under a magnification of 400. The photographs were taken both under crossed and uncrossed polaroids.

The X-ray analysis was done by taking powder patterns in Debye Scherrer cameras, and by taking X-ray diffractograms. Oxide powders for taking film patterns were obtained during descaling procedure mentioned above. Powders of pure alloy were obtained by cutting the alloy ingots with jewel saw.

The powder patterns were taken employing copper target and nickel filter, KV/ mA of 25/15 was used. Samples were

normally rotated during X-ray exposure. Both big (11.46 cm) and small (5.73 cm) cameras were used. The exposure time varied from 9 to 11 hours for the small camera and from 16 to 28 hours for the big camera.

X-ray diffractogram on one sample, viz. Sample seven, was taken exposing the descaled substrate to the X-ray beam. It was done mainly to observe any change in the characteristics of the alloy substrate after oxidation. The diffractograms were also taken on oxide surfaces of those samples which were oxidized at temperatures below 500°C. The diffractograms were taken using copper target and nickel filter.

Microhardness measurements were taken on Tukon hardness tester. Knoop Hardness values of the hardness were measured. The Knoop indenter was pyramidal in form giving a diamond shaped (rhombohedral) indentation of which the diagonals had an approximate relation of 7 to 1. The load of indentation was kept at 1 Kg.

The result of the test was expressed as Knoop Hardness Number (KHN) which relates the applied load in Kg to the unrecovered (approximate) projected area in sq. mm.

The hardness number corresponding to a measured length 'l' of the long diagonal of the indentation for a load of 1 Kg. was obtained from its table.

Hardness measurements were taken on annealed and unannealed samples, on oxidized and unoxidized samples. For



oxidized samples, measurements were taken on oxide surface as well as on bare, descaled substrate. Hardness values were measured on strategic locations on the specimen surface. Thus, values were measured on edges of the sample as well as on its interior. Hardness values on the junctions consisting of oxide scale and bare stripped surface were measured after gradient polishing of the junction region.

In addition to the above measurements, a differential thermal analysis was made with one of the alloy powder samples employing the du Pont 900 analyser. The powder obtained after this analysis was also analysed by X-ray method.



## CHAPTER 3

### THERMOGRAVIMETRY

Description of the samples employed in this investigation is given in Table 1 and Table 2, <sup>The</sup> the samples have been classified in 3 categories based on duration of oxidation and history of the samples. In Table 2, the surface area of the samples exposed to reaction during oxidation, temperature of oxidation, medium of oxidation, time period, along with the final weight gain in  $\text{mg}/\text{cm}^2$  etc. have been given.

Table 2

Basic Information about the Samples

Sample	Surface area ( $\text{cm}^2$ )	Specimen Thickness (cm)	Medium of oxidation	Temperature of oxidation ( $^{\circ}\text{C}$ )	Duration of oxidation (min.)	Final weight gain w ( $\text{mg}/\text{cm}^2$ )
I	3.296	0.08	Oxygen	557	934	1.541
II	1.269	0.04	Air	565	1013	3.096
III	5.944	0.04	Air	276	2245	0.034
IV	2.576	0.04	Air	396	777	0.093
V	1.960	0.10	Air	494	812	0.281
VI	1.328	0.04	Air	550	840	1.054
VII	1.755	0.056	Air	670	537	5.453
VIII	1.215	0.045	Air	537	826	-
1	1.989	0.15	Oxygen	670	93	1.659
2	2.525	0.08	Air	770	78	6.436

Table 2 contd...

3	1.732	0.08	-	-	-	-
4	1.732	0.10	Oxygen	554	240	0.866
5	1.638	0.10	Air	690	99	2.131
6	1.828	0.20	Oxygen	561	360	1.203
7	1.568	0.13	Air	672	111	1.818
8	1.178	0.05	Oxygen	664	030	0.619
9	1.420	0.06	Air	788	73	6.570
10	1.097	0.10	Oxygen	738	20	1.595
11	1.177	0.10	Oxygen	746	85	6.032
12	1.132	0.10	Oxygen	563	90	0.495
13	1.016	0.10	Air	860	36	8.415
14	0.704	0.04	Oxygen	852	27	12.074
15	1.353	0.01	Oxygen	869	5	1.774
one	0.372	0.018	-	-	-	-
two	0.595	-	Oxygen	840	13	2.689
three	0.610	0.068	Oxygen	834	59	15.246
four	0.556	0.02	Air	843	9	2.788
five	0.423	0.024	-	-	-	-
six	0.777	0.042	Oxygen	738	132	10.296
seven	0.887	0.086	Oxygen	595	150	0.733
eight	0.657	0.046	Oxygen	746	18	1.172
nine	0.505	0.026	Air	742	34	1.881
ten	0.943	0.10	Oxygen	611	410	2.598
eleven	0.626	0.024	-	-	-	-

As it is clear from Table 1 and Table 2, the temperature of oxidation varied from a minimum of 276°C for Sample III to a maximum of 869°C for Sample 15. Time period for which the Samples were exposed at various temperatures varied from 5 minutes for Sample 15 to 2245 minutes for Sample III. The final weight gain in  $\text{mg/cm}^2$  was minimum of 0.034 for Sample III to a maximum of 15.246 for Sample three.

The thermogravimetric data for the various samples have been given in Table 3. Table 4 shows trend of variation

of  $n$  in the equation  $w = kt^n$ . The value of  $n$  varied depending on temperature and time of oxidation. Fig. 3-5 give linear plots and Fig. 6-9 log-plots of the thermogravimetric data. Fig. 10 gives Arrhenius plot.

Table 3  
Thermogravimetric Data

Table 3.1				Sample I			
t (min)	m (mg)	t (min.)	m (mg)	t (min.)	m (mg)	t (min.)	m (mg)
0	0	2	0.27	4	0.40	6	0.48
8	0.54	10	0.62	12	0.69	14	0.73
16	0.79	20	0.88	24	0.96	28	1.03
32	1.10	24	1.13	38	1.2	42	1.25
46	1.3	50	1.35	58	1.36	60	1.36
65	1.48	72	1.53	79	1.58	94	1.82
109	1.92	484	3.52	669	4.11	789	4.6
934	5.08	-	-	-	-	-	-

Table 3.2				Sample II			
0	0	1	0.01	2	0.05	3	0.06
4	0.09	5	0.13	6	0.14	7	0.15
8	0.15	9	0.16	10	0.18	11	0.19
12	0.22	14	0.25	16	0.26	18	0.28
20	0.33	21	0.35	26	0.35	28	0.38
30	0.39	32	0.43	34	0.46	36	0.48
38	0.49	41	0.49	42	0.50	44	0.51
48	0.54	68	0.56	86	0.61	90	0.66
108	0.79	126	0.84	160	0.91	198	1.01
231	1.10	261	1.19	288	1.31	318	1.41
349	1.50	379	1.53	506	2.11	560	2.29
620	2.47	680	2.55	745	2.96	798	3.20
870	3.53	926	3.71	978	3.79	1013	3.93

Table 3.3				Sample III			
0	0	8	0	10	0.01	195	0.10
197	0.11	255	0.11	320	0.12	375	0.12

Table 3 contd....

442	0.13	490	0.13	735	0.14	960	0.14
1185	0.14	1551	0.19	1874	0.19	2245	0.120

Table 3.4

Sample IV

0	0	17	0	19	0.01	21	0.02
22	0.04	23	0.05	25	0.05	27	0.06
29	0.06	31	0.07	33	0.07	45	0.07
49	0.08	55	0.08	57	0.09	59	0.10
63	0.10	77	0.10	87	0.11	367	0.12
383	0.14	777	0.24				

Table 3.5

Sample V

0	0	2	0.01	4	0.02	6	0.03
8	0.04	10	0.045	12	0.050	14	0.05
16	0.055	18	0.060	20	0.07	22	0.08
26	0.08	28	0.09	30	0.10	32	0.10
36	0.11	38	0.12	40	0.13	42	0.13
46	0.14	50	0.14	52	0.15	56	0.15
58	0.16	60	0.17	62	0.18	64	0.19
66	0.20	68	0.1	70	0.23	74	0.23
76	0.24	80	0.25	82	0.25	86	0.255
88	0.260	90	0.275	92	0.275	102	0.280
112	0.30	122	0.32	132	0.34	142	0.35
182	0.35	192	0.36	213	0.39	222	0.41
226	0.42	247	0.43	287	0.46	298	0.47
332	0.47	342	0.48	361	0.50	392	0.55
408	0.55	788	0.55	812	0.55		

Table 3.6

Sample VI

0	0	2	0.02	10	0.15	35	0.15
66	0.23	136	0.47	194	0.47	257	0.57
327	0.74	419	0.92	483	0.97	616	1.15
750	1.15	786	1.25	840	1.40		

Table 3.7

Sample VII

0	0	2	0.22	4	0.42	6	0.52
8	0.62	10	0.71	12	0.72	14	0.78
16	0.82	18	0.90	20	0.92	22	0.97
24	1.02	26	1.02	28	1.10	30	1.12

Table 3 contd...

t	m	t	m	t	m	t	m
32	1.12	34	1.17	40	1.17	50	1.22
52	1.22	54	1.25	56	1.27	58	1.31
60	1.32	62	1.327	79	1.440	92	1.62
131	2.12	183	3.07	213	3.47	244	3.87
277	4.42	307	5.02	346	5.80	368	6.27
397	6.67	428	7.37	451	7.87	517	9.42
537	9.57						

Table 3.8

Sample 1

t	m	t	m	t	m	t	m
0	0	1	0.25	3	0.56	5	0.58
7	0.67	9	0.77	11	0.87	13	0.97
15	1.04	17	1.16	19	1.29	21	1.40
23	1.47	25	1.55	27	1.63	29	1.73
31	1.82	33	1.93	35	2.01	37	2.05
39	2.10	41	2.16	43	2.20	45	2.24
47	2.27	49	2.32	51	2.35	53	2.40
55	2.47	57	2.50	61	2.52	65	2.60
70	2.75	73	2.85	77	2.89	81	2.98
85	3.11	89	3.20	93	3.30		

Table 3.9

Sample 2

t	m	t	m	t	m	t	m
0	0	2	0.60	4	1.11	6	1.56
8	1.90	10	2.23	12	2.55	14	2.90
16	3.25	18	3.65	20	4.00	21	4.40
23*	4.59	25	4.91	27	5.26	29	5.66
31	6.03	33	6.40	35	6.85	37	7.35
39	7.81	41	8.33	42	8.55	44*	8.90
46	9.33	48	9.66	50	10.01	52	10.44
54	10.80	56	11.35	57*	11.49	59	11.92
61	12.30	63	12.75	65	13.12	67	13.53
69	13.92	71	14.37	73	14.87	75	15.38
77	15.90	78	16.25				

\* Sample interrupted as mentioned elsewhere  
 Colour of oxide surface: black at 23 min., white at 44 min.  
 and onwards.

Table 3.10

Sample 4

t	m	t	m	t	m	t	m
0	0	2	0.10	4	0.15	6	0.18
8	0.23	10	0.25	12	0.28	14	0.30
16	0.35	18	0.37	20	0.40	24	0.47
28	0.50	32	0.55	36	0.60	40	0.65

Table 3 contd....

t	m	t	m	t	m	t	m
44	0.67	48	0.70	50	0.75	54	0.77
58	0.83	60	0.83	68	0.86	78	0.94
88	0.98	108	1.09	128	1.18	148	0.25
178	1.35	223	1.49	240	1.50		

Table 3.11

Sample 5

0	0	4	0	6	0.05	8	0.09
10	0.12	12	0.25	14	0.37	16	0.47
20	0.49	20	0.53	22	0.70	24	0.77
26	0.80	28	0.96	30	1.09	32	1.12
34	1.25	36	1.25	38	1.41	40	1.54
42	1.55	44	1.65	46	1.67	48	1.70
50	1.75	52	2.10	56	2.10	58	2.14
62	2.14	64	2.28	65	2.45	66	2.59
70	2.59	72	2.71	74	2.75	76	2.90
78	2.92	80	2.96	82	3.02	84	3.02
86	3.12	88	3.15	90	3.22	92	3.26
94	3.47	98	3.47	99	3.49		

Table 3.12

Sample 6

0	0	2	0.10	4	0.20	6	0.27
8	0.31	10	0.37	12	0.42	14	0.48
16	0.54	18	0.58	20	0.65	22	0.67
24	0.70	26	0.70	28	0.75	30	0.80
32	0.80	34	0.85	36	0.87	38	0.92
40	0.93	42	0.95	44	1.00	58	1.05
60	1.08	64	1.10	80	1.13	90	1.13
125	1.31	155	1.45	185	1.60	240	1.75
290	1.95	325	2.10	360	2.20		

Table 3.13

Sample 7

0	0	2	0.27	4	0.45	6	0.55
8	0.69	10	0.78	12	0.88	14	1.95
16	1.03	18	1.07	20	1.15	22	1.20
24	1.25	26	1.30	28	1.35	30	1.42
32	1.50	34	1.55	36	1.59	38	1.61
40	1.64	42	1.70	44	1.71	46	1.78
48	1.82	50	1.85	52	1.90	54	1.96
56	1.96	58	1.97	60	1.99	62	2.10
64	2.14	66	2.15	68	2.17	70	2.19
74	2.26	78	2.38	82	2.45	86	2.50

Table 3 contd...

t	m8	t	m	t	m	t	m
90	2.54	92	2.55	94	2.55	96	2.60
98	2.65	100	2.67	102	2.70	104	2.72
106	2.75	108	2.82	111	2.85		

Table 3.13

Sample 8

0	0	2	0.05	4	0.15	6	0.20
8	0.27	10	0.33	12	0.40	14	0.43
16	0.47	18	0.50	20	0.55	22	0.56
24	0.56	26	0.65	28	0.70	30	0.73

Table 3.15

Sample 9

0	0	2	0.43	4	0.81	6	1.06
8	1.23	10	1.41	12	1.58	14	1.76
16	1.91	18	2.10	20	2.27	22	2.52
24	2.75	26	3.01	28	3.35	30	3.63
32	3.90	34	4.10	36	4.35	38	4.62
40	4.88	42	5.12	44	5.40	46	5.62
48	5.90	50	6.18	52	6.47	54	6.78
56	7.00	58	7.30	60	7.60	62	7.86
64	8.10	66	8.41	68	8.67	70	8.93
72	9.22	73	9.33				

Table 3.16

Sample 10

0	0	1	0.20	2	0.37	3	0.52
4	0.67	5	0.75	6	0.87	7	0.95
8	1.02	9	1.07	10	1.14	11	1.18
12	1.25	13	1.29	14	1.36	15	1.40
16	1.45	17	1.53	18	1.60	19	1.68
20	1.75						

Table 3.17

Sample 11

0	0	2	0.32	4	0.55	6	0.71
8	0.82	100	0.93	12	1.02	14	1.10
16	1.20	18	1.32	20	1.43	22	1.52
24	1.62	26	1.75	28	1.89	30	2.02
32	2.15	34	2.30	36	2.44	38	2.55
40	2.75	42	2.91	44	3.07	46	3.27
48	3.50	50	3.71	52	3.95	54	4.16
56	4.40	48	4.59	60	4.75	62	4.94
64	5.02	66	5.43	68	5.51	70	5.70
72	5.89	74	6.00	76	6.32	78	6.51
80	6.71	82	6.93	84	7.05	85	7.10



Table 3 contd...

t	m	t	m	t	m	t	m
Table 3.18		Sample 12					
0	0	2	0.18	4	0.22	6	0.26
8	0.29	12	0.29	14	0.31	16	0.35
18	0.35	24	0.36	30	0.42	36	0.44
40	0.46	50	0.47	60	0.48	75	0.51
90	0.56						

Table 3.19		Sample 13					
0	0	1	0.30	2	0.63	3	0.85
4	1.00	5	1.21	6	1.40	7	1.58
8	1.73	9	1.85	10	2.05	11	2.30
12	2.50	13	2.80	14	3.23	15	3.56
20	5.20	21	5.50	22	5.76	23	6.05
24	6.40	25	6.81	26	7.00	27	7.30
28	7.55	29	7.82	30	8.05	31	8.25
32	8.30	33	8.32	34	8.36	35	8.40
36	8.55						

Table 3.20		Sample 14					
0	0	1	0.15	2	2.31	3	0.45
4	0.55	5	0.65	6	0.91	7	1.19
8	1.42	9	1.75	10	2.06	11	2.30
12	2.60	13	2.90	14	3.20	15	3.50
16	3.85	17	4.20	18	4.56	19	4.90
20	5.30	21	5.68	22	6.20	23	6.60
24	7.08	25	7.55	26	8.01	27	8.50

Table 3.21		Sample 15					
0	0	1	0.65	2	1.08	3	1.45
4	1.90	5	2.40				

Table 3.22		Sample two					
0	0	1	0.18	2	0.30	3	0.41
4	0.47	5	0.60	6	0.70	7	0.75
8	0.85	9	0.94	10	1.07	11	1.15
12	0.30	13	1.60				

Table 3.23		Sample three					
0	0	1	0.17	1	0.25	2	0.30
3	0.38	4	0.42	5	0.50	6	0.55
7	0.61	8	0.68	9	0.72	10	0.83



Table 3 contd...

t	m	t	m	t	m	t	m
11	0.90	12	1.01	13	1.15	14	1.33
15	0.45	16	1.75	17	1.64	18	1.72
19	1.82	20	1.96	21	2.05	22	2.16
23	2.31	24	2.43	25	2.60	26	2.70
27	2.80	28	2.95	29	3.11	30	3.29
31	3.47	32	3.66	33	3.95	34	4.07
35	4.28	36	4.50	37	4.66	38	4.81
39	5.02	40	5.26	41	5.43	42	4.65
43	5.85	44	6.11	45	6.34	46	6.55
47	6.80	48	7.01	49	7.21	50	7.40
41	7.46	52	7.73	53	7.95	54	8.20
55	8.50	56	8.60	57	8.90	59	9.30

Table 3.24

Sample four

0	0		0.15	1	0.28	2	0.33
3	0.40	4	0.51	5	0.71	6	0.82
7	0.96	8	1.35	9	1.55		

Table 3.25

Sample six

0	0	2	0.05	4	0.15	6	0.20
8	0.26	10	0.30	12	0.36	14	0.47
16	0.53	18	0.62	20	0.70	22	0.80
24	0.87	26	0.96	28	1.06	30	1.16
32	1.23	34	1.33	36	1.44	38	1.58
40	1.70	42	1.80	44	1.90	46	1.95
48	2.05	50	2.17	52	2.31	54	2.45
56	2.58	58	2.67	60	2.81	62	2.90
66	3.20	70	3.50	74	3.72	78	4.05
82	4.34	86	4.62	90	4.93	94	5.20
98	5.50	100	5.65	104	5.93	108	6.22
112	6.50	116	6.83	120	7.12	124	7.40
128	7.68	132	8.00				

Table 3.26

Sample seven

0	0	2	0.10	4	0.20	6	0.21
8	0.25	10	0.26	20	0.31	30	0.31
60	0.31	70	0.40	100	0.47	130	0.60
150	0.65						

Table 3.27

Sample eight

0	0	1	0.13	2	0.19	3	0.25
4	0.30	5	0.35	6	0.38	7	0.45
8	0.48	9	0.52	10	0.55	11	0.55
12	0.56	13	0.57	14	0.60	15	0.63

Table 3 contd...

t	m	t	m	t	m	t	m
15	0.68	17	0.74	18	0.77		

Table 3.28

Sample nine

0	0	2	0.10	4	0.16	6	0.18
8	0.20	10	0.24	12	0.30	14	0.31
16	0.35	18	0.39	20	0.43	22	0.48
24	0.55	26	0.64	28	0.67	30	0.76
32	0.86	34	0.95				

Table 3.29

Sample ten

0	0	2	0.01	4	0.02	6	0.09
8	0.12	10	0.15	12	0.18	14	0.22
16	0.25	18	0.27	20	0.30	22	0.32
24	0.35	26	0.38	28	0.40	30	0.40
35	0.41	40	0.45	45	0.50	55	0.50
65	0.55	91	0.65	129	0.65	159	0.80
189	0.00	217	1.20	148	1.40	278	1.55
308	1.75	315	2.00	410	2.45		

### 3.1 Reproducibility of the Thermogravimetric Results:

A study of Fig. 3-5 suggests that the weight gain curves are fairly reproducible for initial stages of oxidation. As an evidence to it, Fig. 5 shows that oxidation behaviour of Samples two and three which were oxidised at around 840°C in oxygen is identical in the initial stages and deviation occurs only after a considerable time of oxidation is elapsed.

For initial stages, the above observations thus suggest that the weight gain curves are quite reproducible. However, for extended oxidation reproducibility is less due probably

to the unpredictable behaviour of niobium associated with the modifications of its oxides and interaction with other constituents present.

Some variations in reproducibility in the initial stages can be attributed to the varying metallurgical conditions of the different specimen surfaces. To name a few, varying surface roughness has been associated with discrepancies observed in oxidation of many metals. Remanence of etching-chemicals, particularly those containing fluorine as in our case, can have large effect. Though care was taken in the present investigation to remove every trace of chemicals by washing the etched specimen in running tap water for about half an hour, possibility of any entrapped quantity can not be ignored. In this connection, it may be of interest to note that Amsel et al.<sup>61</sup> recently observed while analysing zirconium metal surfaces that chemical polishing in  $\text{HF-HNO}_3$  bath caused formation of a thin layer of oxide. The process did not, however, introduce oxygen into solid solution with the underlying metal. Effect of F-ions should be expected to decrease corrosion rate if it enters in monovalent form to dissolve by substitution in  $\text{ZrO}_2$  scale according to the mechanism proposed. However, nature of its interaction with the oxide is not known.

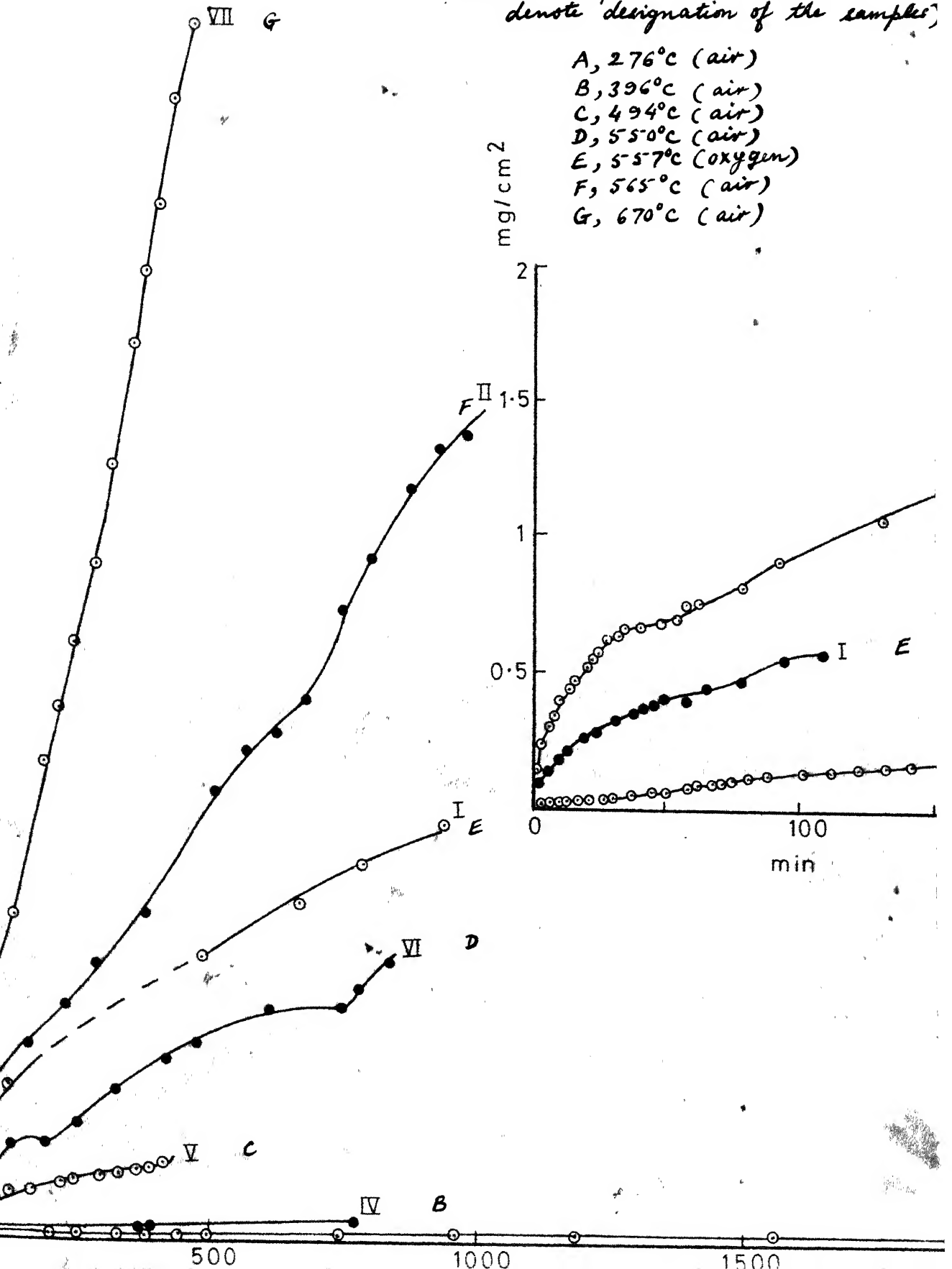
### 3.2 Effect of Thermal Cycling:

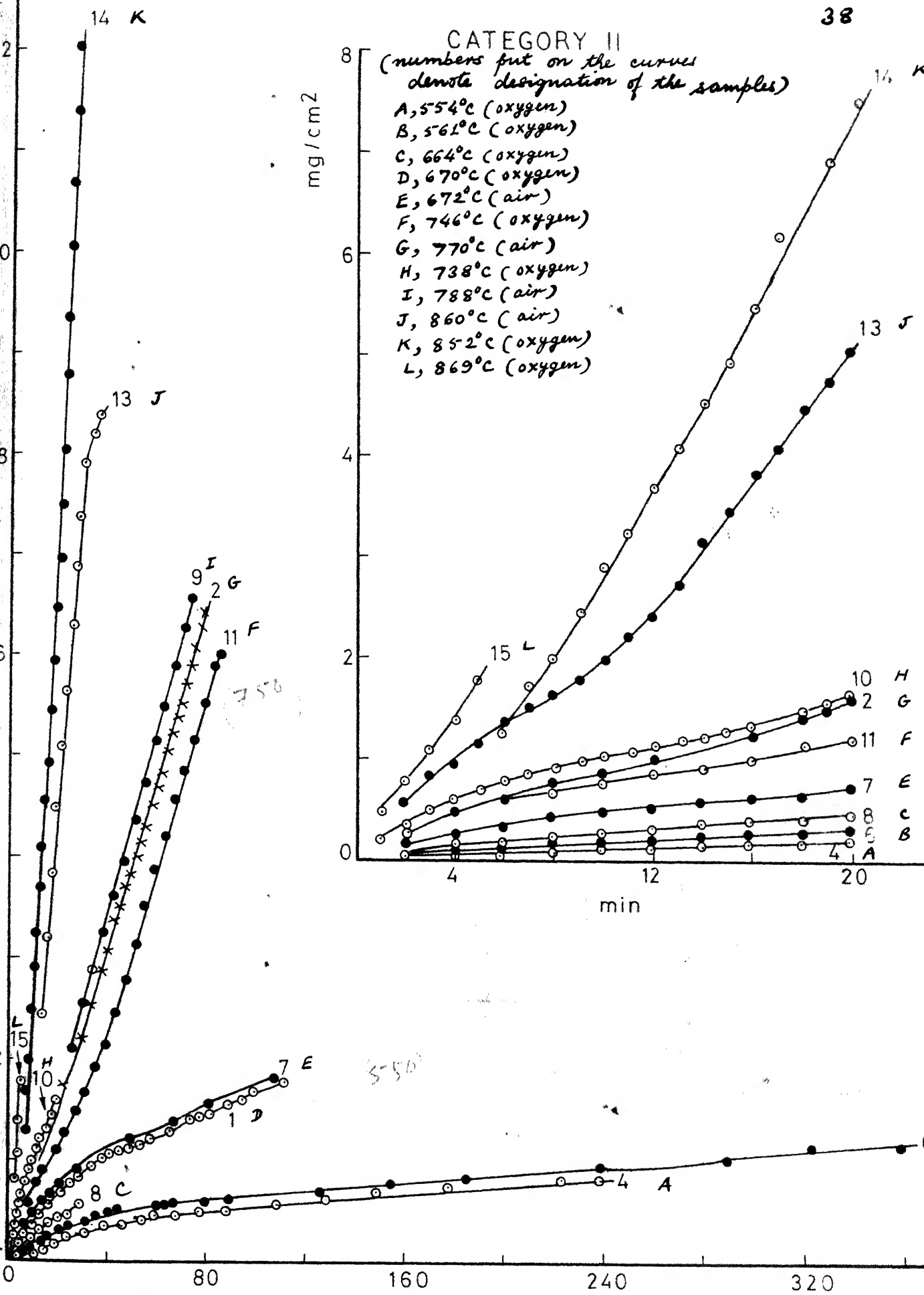
Sample 2, during its 78 minute - oxidation run was

## CATEGORY I

(numbers put on the curves denote designation of the samples)

- A, 276°C (air)  
 B, 396°C (air)  
 C, 494°C (air)  
 D, 550°C (air)  
 E, 557°C (oxygen)  
 F, 565°C (air)  
 G, 670°C (air)

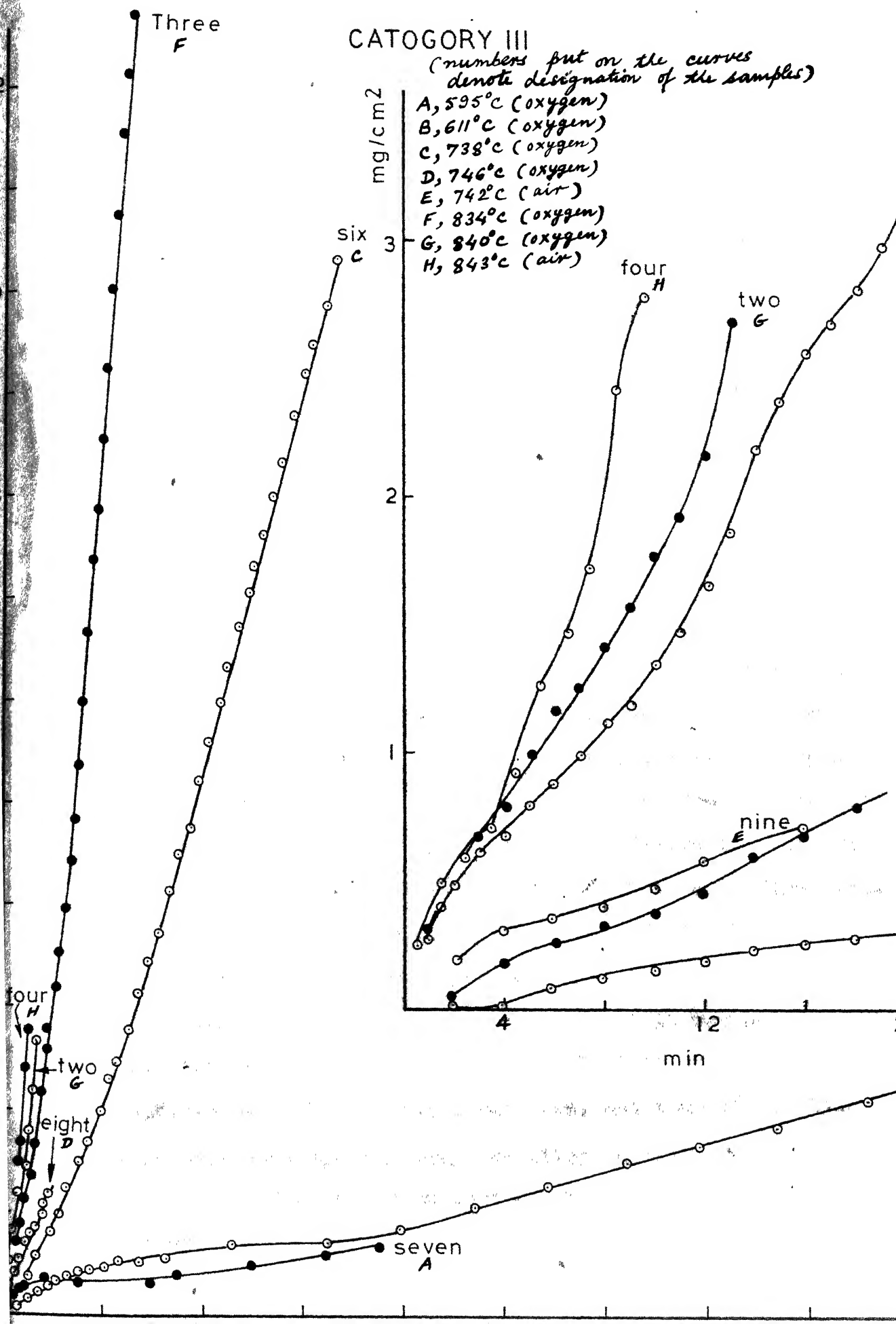




# CATOGORY III

(numbers put on the curves denote designation of the samples)

- A, 595°C (oxygen)
- B, 611°C (oxygen)
- C, 738°C (oxygen)
- D, 746°C (oxygen)
- E, 742°C (air)
- F, 834°C (oxygen)
- G, 840°C (oxygen)
- H, 843°C (air)



interrupted thrice at 23 min., 44 min. and 57 min. by cooling down the sample each time to room temperature and subsequently subjected it to the same temperature again for further reaction.

It is obvious from Fig. 4 that weight gain curve for Sample 2 does not apparently exhibit any discontinuity at the points where the sample was interrupted. This suggests little effect of thermal cycling in this respect.

### 3.3 Effect of Temperature and Time:

The low temperature measurements such as for Samples III and IV oxidized at 276 and 396°C respectively could not be taken with great accuracy. It appears from log-plot in Fig. 7 that the rate law for the oxidation of these samples is perhaps logarithmic. At higher temperatures, it appears from thermogravimetric curves that the rate law is parabolic or linear depending on temperature and elapsed time of oxidation. There is also substantial deviation of  $n$  from parabolic or linear behaviour as given in Table 4. The rate law was, however, not found cubic in any of the temperature and time ranges studied. In this connection, it may be pointed out that the literature survey reveals that pure zirconium oxidizes according to cubic rate law, and thus observation made with Zr - 2.5 wt. pct. Nb alloy in this work points out a deviation from  $n = 3$  in contrast to the case of pure zirconium.

As expected, Table 4 shows that with increasing temperature value of the rate constant  $k$  in equation  $w^n = kt$ , and hence the weight gain, increases in general.

Table 4  
Variation of  $n$  and  $k$  in  $w^n = kt$

Sample	Time interval for which $n$ holds (min.)	$n$	$k$ (mg/cm <sup>2</sup> ) <sup><math>n</math></sup> /min. ( $\times 10^4$ )
I	< 60	2	39.81
	60 - 500	2.2	
	> 500	1.5	
II	< 80	?	35.48 31.62
	80 - 400	2	
	> 400	1	
III	Upto 2245	log(?)	
IV	Upto 777	log(?)	
V	< 70	?	1.288
	200-410	2	
VI	< 750	?	1in
	> 750	1in	
VII	< 30	2	144.5
	30 - 120	?	93.3
	> 120	1	
2	< 12	1.3	831.8
	> 12	1	
4	< 50	1.6	42.66
	> 50	2	31.62
6	< 10	1.5	79.43
	11-20	1.4	
	20-50	1.9	
	50-90	?	
	> 90	2	
			40.74



Table 4 contd...

7	< 10	1.5	398.1
	10-40	1.7	
	> 50	2	281.8
8	< 13	1	251.2
	> 13	1.8	125.9
11	< 13	2	631.0
	13-26	1.4	
	26-50	1	501.2
	> 50	0.75	478.6
14	< 5	0.9	1660
	> 6	0.7	2042
15	Upto 5	1.1	3715
two	< 5	1.5	1622
	> 5	0.8	2089
three	< 9	1.9	1413
	9 - 27	0.8	1000
	> 27	0.7	
four	< 4	2	1288
	4 - 8	0.8	2188
	> 8	0.5	
six	< 11	1	28818
	> 11	0.75	436.5
nine	< 8	2	229.1
	8-16	1	426.6
	> 16	0.8	436.5
ten	< 27	1	
	27 - 140	2.6	
	> 140	1	54.95

---

As mentioned earlier and shown in Table 4, it is clear that the value of n varied with temperature and time. At low temperature oxidation, such as for the case of

Sample V, VII in category I, 6 in category II and ten in category III oxidized at 494, 670, 561 and 611°C respectively, it is seen from this table as well as from the double -log plots in the Fig. 6, 8 and 9 that increase in the value of  $n$  is found after initial change in oxidation kinetics. A decrease in oxidation rate has often been observed for the case of pure niobium<sup>35,62,63</sup> with increasing temperature at around 600°C, and has been thought to result from sintering of the scale. The decrease in oxidation rate after some elapsed time of oxidation in the present case may also be thought to be due to a change in plasticity of the oxide.

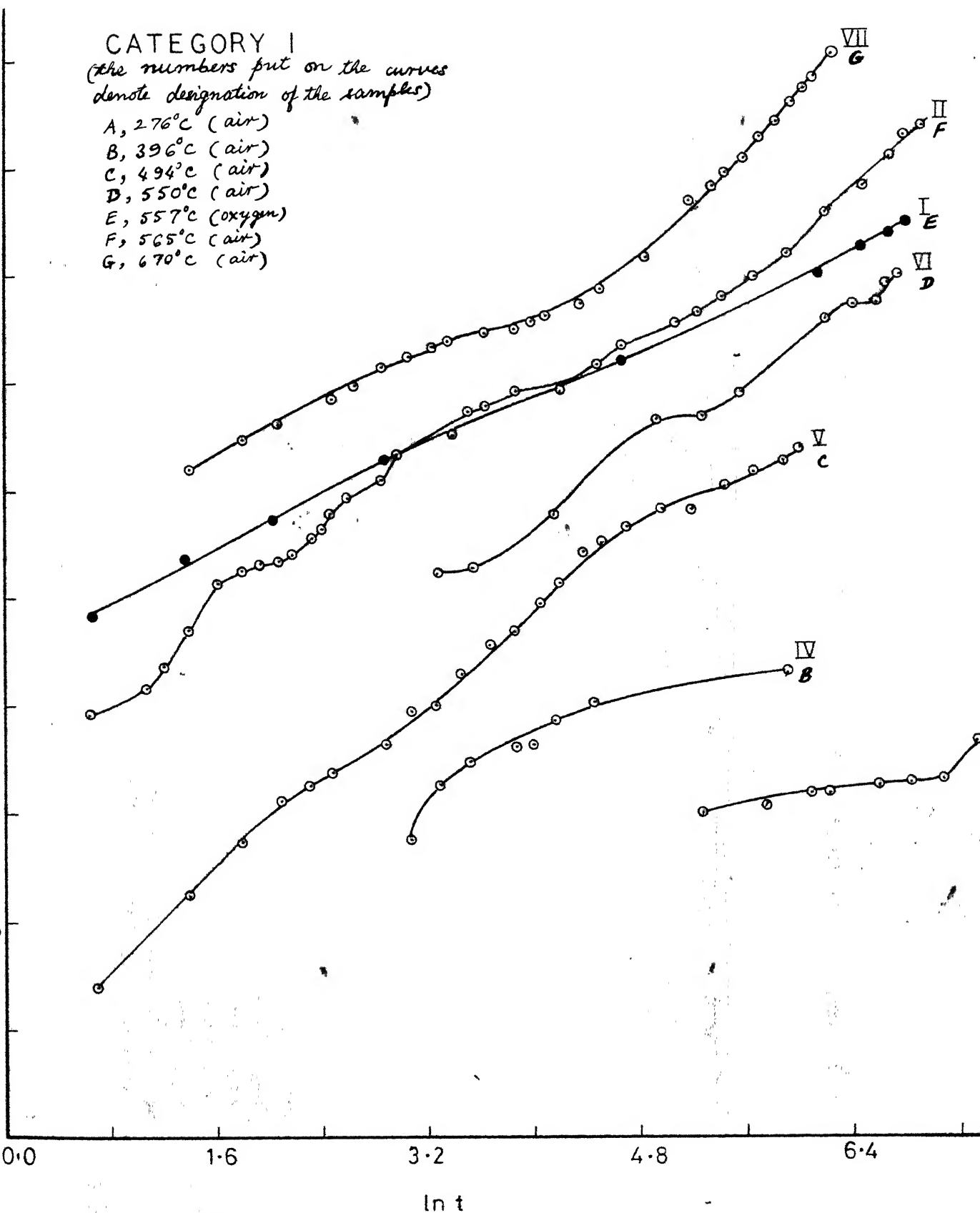
At high temperature oxidation such as at temperatures employed for oxidation of Sample Six (738°C) and three (834°C), it is obvious from Fig. 9 that the value of  $n$  decreases after initial change in kinetics. It indicates that kinetics changes to enhanced rate of oxidation with elapsed time at these temperatures.

As mentioned earlier, the oxidation of pure zirconium possibly follows a cubic rate law, but it is observed from the present work (see Table 4) that Zr -2.5 wt. pct. Nb alloy does not oxidize according to this and  $n$  was always found to be less than 3. A corresponding parabolic law has been observed in general. In this connection, it may be mentioned for the sake of comparison that the same rate law (i.e. parabolic) was observed by Dawson et al.<sup>64</sup> for the oxidation of its close competitor zircaloy - 2 in oxygen at 300 - 360°C.

## CATEGORY I

(the numbers put on the curves denote designation of the samples)

- A, 276°C (air)
- B, 396°C (air)
- C, 494°C (air)
- D, 550°C (air)
- E, 557°C (oxygen)
- F, 565°C (air)
- G, 670°C (air)



6 - Double Log. Plot of Oxidation Data for the Samples in Cat. I

# CATEGORY I

(The numbers put on the curves denote designation of the samples)

- A, 276°C (air)
- B, 396°C (air)
- C, 494°C (air)
- D, 550°C (air)
- E, 565°C (air)

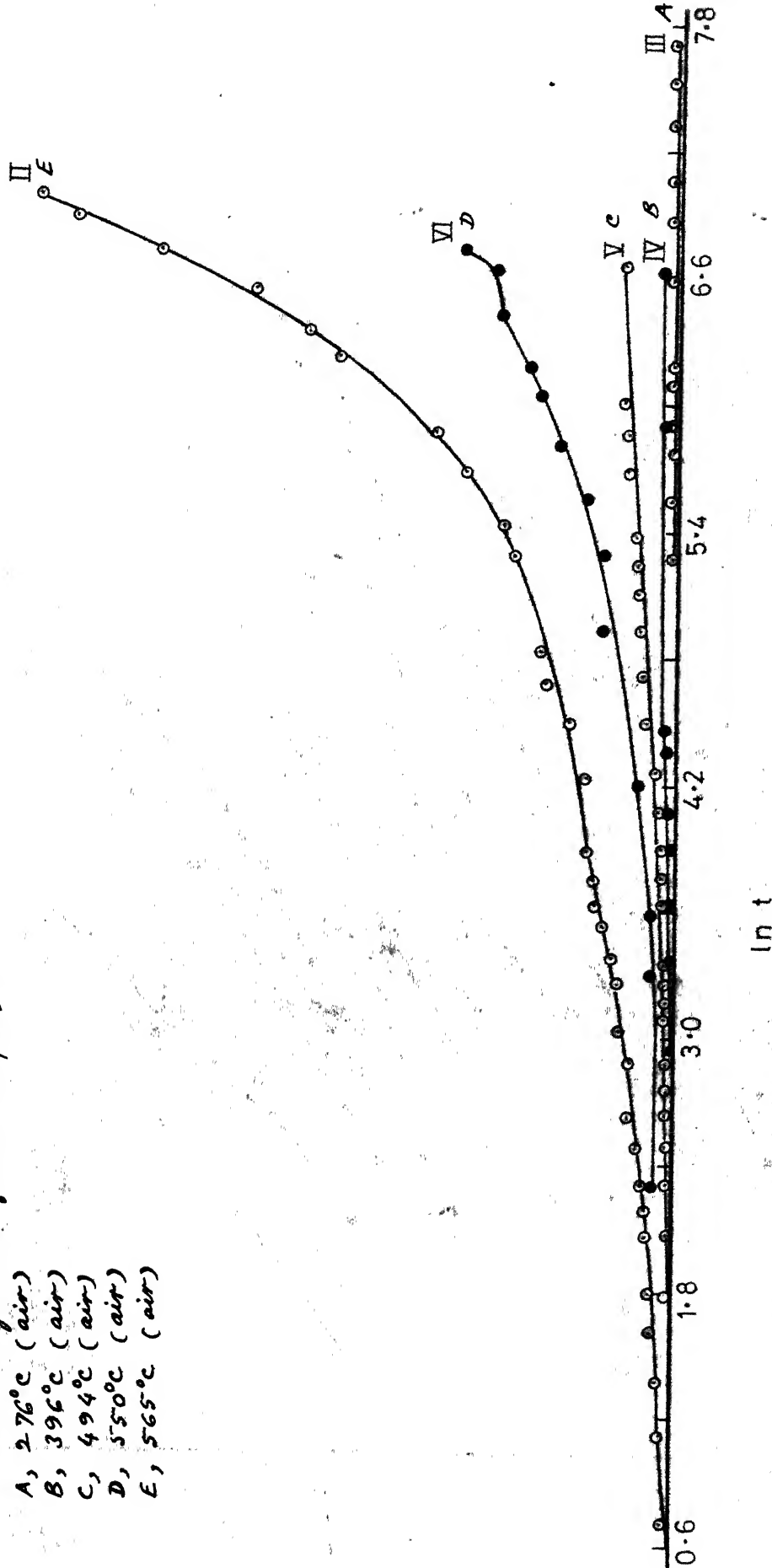
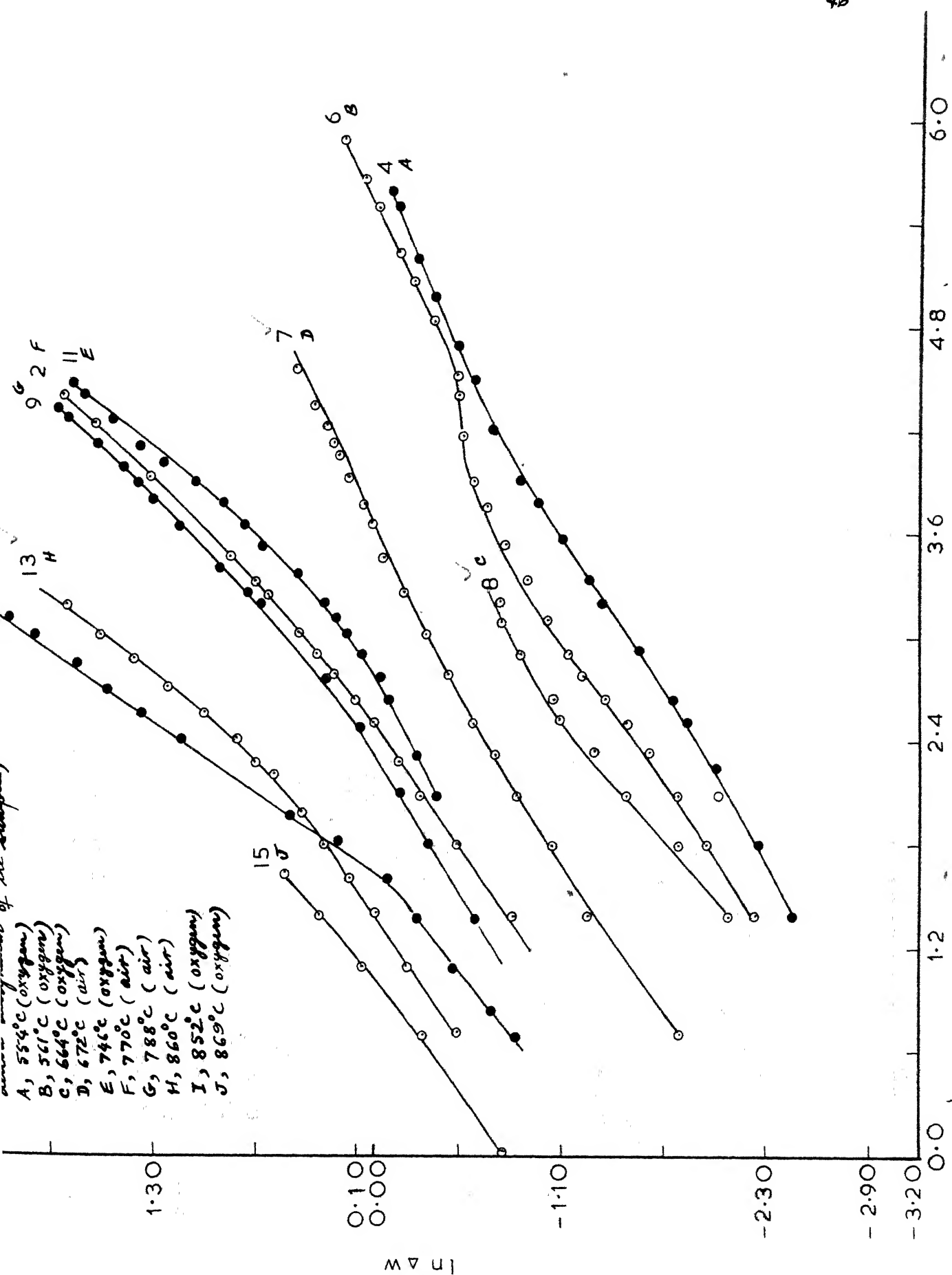
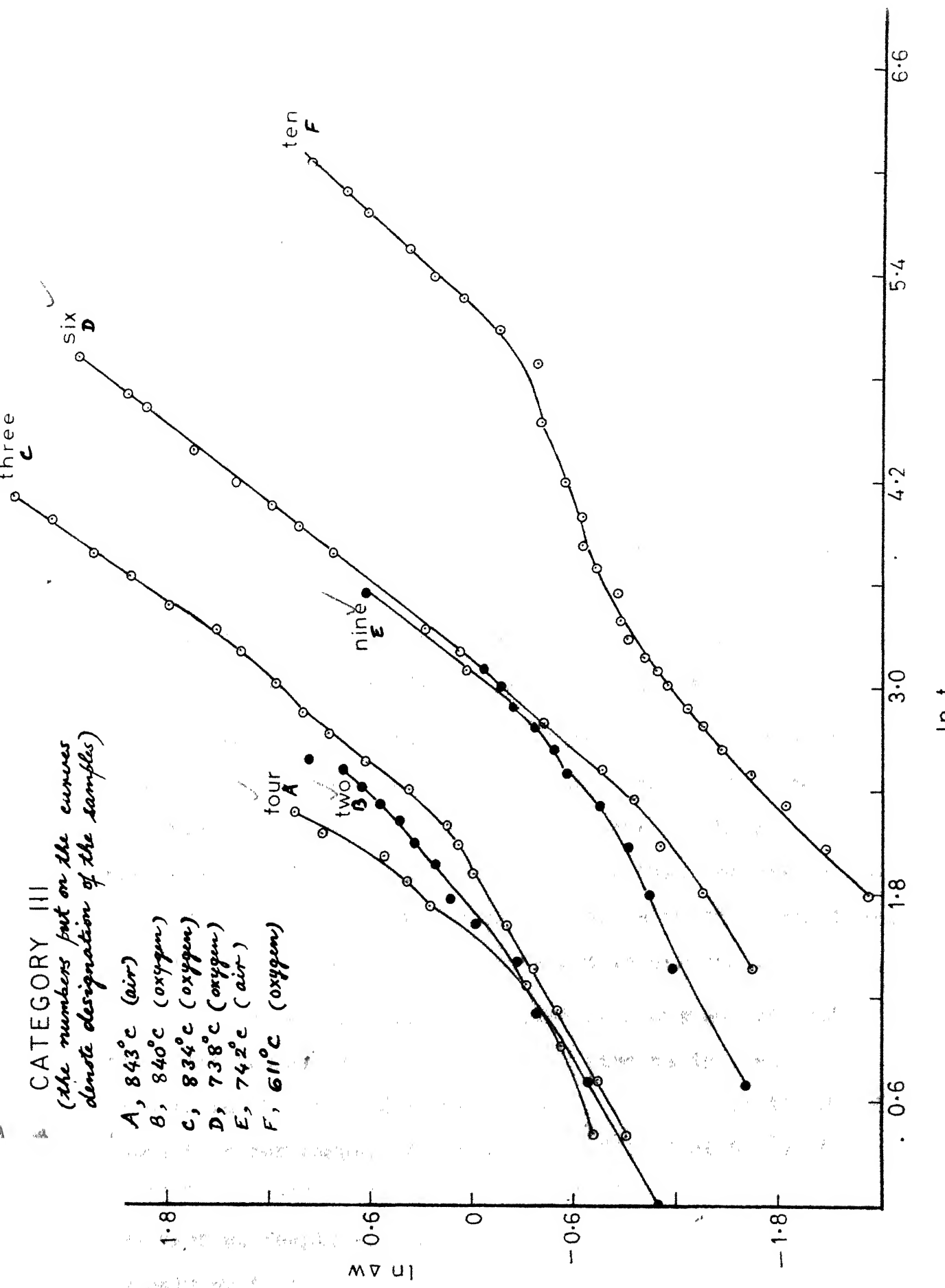


Fig. 7 - Single Log. Plot of Oxidation Data for the Samples in Cat. I



CATEGORY III  
(the numbers put on the curves  
denote designation of the samples)

- A, 843°C (air)
- B, 840°C (oxygen)
- C, 834°C (oxygen)
- D, 738°C (oxygen)
- E, 742°C (air)
- F, 611°C (oxygen)



The mechanism associated with the parabolic law will be taken in section 3.4.

Fig. 3-5 show that the change in kinetics of oxidation leads to appearance of a number of cycles in the weight-gain curves. It appears from these figures that at any given temperature of oxidation the occurrence of transition seems to take more and more time as the oxidation time elapses. As an evidence to it, Sample II in Fig. 3 shows a rate transition at around 200 min. and the next transition occurs at around 700 min. Similarly Fig. 4 indicates that for Sample 13 while a transition has occurred at around 8 min., the next transition has not yet started after 20 min. have elapsed.

Reason for increased time taken for the progressive transitions may be attributed to some extent to the increased thickness of the oxide layer. As suggested by Koifstad, a possibility exists for the porous scales that the gas diffusion through the pores may play a role, in reaction kinetics. This may lead to a prolonged <sup>transition</sup> oxidation in our case.

It is obvious from the weight-gain curves (Fig.3-5) that with increasing temperature the time to initial transition in the kinetics decreases. As an evidence to it, Fig.5 shows that for Sample ten which was oxidized at  $611^{\circ}\text{C}$  the initial transition occurred at around 120 min. whereas for the case of Sample six which was oxidized at  $738^{\circ}\text{C}$  this time is only at 8 min.

An early appearance of stoichiometric white oxide with the associated porosity of it appears to contribute to such decrease in transition time with the increasing temperature.

The weight-gain curves also show that with increasing temperature the number of cycles for the same thickness of oxide formed decreases. Thus Sample VII which was oxidized at  $670^{\circ}\text{C}$  shows less number of cycles when compared with Sample II and VI which were oxidized at  $555^{\circ}\text{C}$  and  $565^{\circ}\text{C}$  respectively, (see Fig. 3).

The fact that oxidation of pure zirconium does not lead to occurrence of such transition cycles indicates that oxides of niobium are responsible for such observation with the case of present alloy. Thus the appearance of a lower number of transition cycles with increasing temperature may be associated with some modification of niobium oxide taking place as temperature increases.

### 3.4 Mechanism of Oxidation:

The different kinetics of oxidation leading to variation in values of  $n$  in equation  $\Delta w^n = kt$  as shown in Table 4 may be ascribed to different mechanisms.

The low temperature oxidation study made at  $276$  and  $396^{\circ}\text{C}$  for Sample III and IV respectively appears to indicate that logarithmic rate law is obeyed for such low temperature oxidation. The mechanism of this oxidation behaviour is not



clearly understood. Fig. 7, which gives straight lines when  $w$  is plotted against  $\ln t$  for Sample III and IV, appears to suggest that oxidation kinetics for these samples obeys the equation  $w = k \ln t + c$ . This equation indicates direct logarithmic oxidation. Such a direct logarithmic law of oxidation was derived by Mott in 1940 assuming electron tunneling through the thin oxide film to be the rate determining step of oxidation.

Values of  $n$  given in Table 4 show that when a thick oxide film has formed, a parabolic rate law with  $n = 2$  follows. The diffusion of oxygen ions through O-vacancies in  $ZrO_2$  scale seems to be rate determining step of oxidation according to Wagner's mechanism. Oxygen may also diffuse through oxide of niobium supposed to be present in the scale.

A slight deviation from  $n = 2$  listed in Table 4 may be accounted for the change in composition of the constituents of this alloy phase on its surface. This is in agreement with the hypothesis proposed by Heindlhofer and Larsen<sup>65</sup> according to which no alloy can be expected to oxidize exactly in proportion to  $\sqrt{t}$  at constant temperature, because the condition that the composition of the alloy immediately adjacent to the scale remains constant with time is not likely to hold in view of the differences in the rates of oxidation of the component metals and in the oxygen pressures of the oxides.

This seems to be correct when the first stages of oxidation are considered. After some time when stationary equilibrium is established, the concentration at the alloy/oxide interface may usually be taken to be constant:

The mechanism proposed for parabolic oxidation presumes presence of oxygen vacancies in the scale. The literature, however, reveals that the exact nature of defects is not known. While  $\text{Nb}_2\text{O}_5$  is commonly accepted to consist of oxygen vacancies, there are doubts about the type of defects in  $\text{ZrO}_2$  scale. The presence of O-defects had been accepted by many investigators which include Chirigos and Thomas,<sup>66</sup> Porte et al.<sup>15</sup> and Douglass.<sup>67</sup>

Chirigos and Thomas<sup>66</sup> confirmed diffusion of O-ions through O-vacancies by marker experiment. This was in agreement with the observation of Porte et al.<sup>15</sup> that the cubic rate law for oxidation of zirconium was independent of pressure. A further evidence about the mechanism of oxidation governed by O-diffusion in the parabolic range is substantiated by the fact that the value of activation energy for parabolic oxidation in the present investigation (viz. 37.5 kcal/mol) is in agreement with the activation energy of 33 kcal/mole obtained by Douglass<sup>67</sup> for O-diffusion in  $\text{ZrO}_2$ . From this, one may conclude that O-diffusion is the rate controlling step of oxidation.

The mechanism based on O-vacancies in  $\text{ZrO}_2$  has been adopted to account for the variation in oxidation behaviour

observed in air and oxygen media in the present investigation. The effect of air and oxygen will be taken in section 3.5. Here it must be pointed out that while the investigations of Chirigos and Thomas, Porte et al. and Douglass mentioned above justify the presence of O-deficits in the zirconia scale, there is an increasing uptrend to hold a different opinion about the defect type, Vest et al.,<sup>68</sup> in a study of electrical conductivity of  $\text{ZrO}_2$  scale as a function of oxygen pressure at  $990^\circ\text{C}$  found a minimum at about  $10^{-16}$  atm. oxygen, suggesting a transition from n to p type conductivity. At high oxygen pressure such as 1 atm., dependence of electrical conductivity with oxygen pressure ( $\sigma \propto p\text{O}_2^{1/5}$ ) was interpreted in terms of Zr - vacancies.

Table 4 shows value of n in equation  $w^n = kt$  to be equal to 1, i.e., linear rate law, at many temperatures occurrence of which also depends on elapsed time of oxidation. Phase boundary reaction at oxide/alloy interface appears to control the reaction. This would occur when the oxide scale does not offer any resistance for direct passage of oxygen through it. The phase boundary reaction then may be controlled by either O-adsorption on the interface or incorporation of O-atoms. In this work because of high pressure of the gas used (1 atm.) the former process is unlikely to control the reaction. Incorporation of O-atoms can then be thought to be rate controlling.

Although possible mechanisms leading to logarithmic, parabolic and linear oxidation have been pointed out above.

it is well known that for any metal or alloy, in general, only the mechanism for parabolic oxidation can be thought to be well understood. For significant deviations from  $n = 2$ , the mechanism is difficult to predict from our present knowledge about the processes occurring during oxidation of metals and alloys.

The occurrence of transition cycles observed in the weight gain curves (see Fig. 3-5) can be associated with intermittent formation of cracks in the oxide offering low resistance to passage of gas through it. The cause leading to crack formation and the resulting change in kinetics will be taken in more details in 'general discussion'. If the formation of intermittent cracks is accepted as a cause for transition cycles, it can be argued on the basis of our observation showing sharp increase in the weight gain at transition as a result of crack formation that the cracks are more difficult to nucleate than to propagate. On this basis it is implied from the occurrence of cyclic behaviour that the cracks are not continuously un-nucleating which would otherwise lead to a persistent linear law after the initial protective behaviour. This argument is based on a proposal of Wanklyn<sup>69</sup> to explain the linear rate law.

### 3.5 Effect of Medium of Oxidation:

Oxidation runs were carried out in air and in oxygen, and the results of their measurements are summarised in Table 3

and shown in Fig. 3-10. From Table 5, it is evident that the oxidation behaviour of the alloy at the same temperature and pressure is different in air and in oxygen. It is clear from Table 5 and Fig. 4-5 that

(a) the initial weight gain is higher for oxidation in the air than for oxidation in pure oxygen.

(b) the difference in weight gain in the initial stages between the two cases of oxidation, i.e. in air and in oxygen, decreases with increasing temperature.

(c) the initial oxidation rate in air appears to be parabolic whereas in case of oxygen it is approaching to a linear law, as indicated from values of  $n$  given in Table 5.

(d) for oxidation beyond initial stages, the reaction kinetics is rather difficult to compare for the two media. This may be probably due to complexities involved with different modifications of oxides of niobium and their interactions with other oxides.

The higher initial weight gain observed for the case of air may be due to substitutional N-atoms in the oxide  $ZrO_2$  resulting in increase in oxygen ion vacancies. This increase in vacancy concentration will increase the oxygen uptake by diffusion leading to parabolic law. From this result in air one can expect that oxidation of the alloy in pure oxygen should also follow parabolic rate. But it

Table 5

Comparison of Initial Kinetics for Oxidation in  
Air and in Oxygen

Air				Oxygen			
Temp. of oxida- tion (°C)	Sample	Initial value of n	Time for which n holds (min.)	Temp. of oxi- dation (°C)	Sample	Initial value of n	Time for which n holds (min.)
672	7	1.5	9	664	8	1	12
860	13	1.5	6	852	14	0.9	5
742	nine	2	8	738	six	1	11
843	four	2	4	840	two	1.5	5

is inconsistent with the present observations as pointed out in (c). It is possible that for a very small period of time, approximately one min. or so, oxidation in oxygen may follow parabolic rate, but soon after a transition to linear rate occurs. This may be possibly due to lower plasticity and accompanied decrease in protectiveness of the scale formed in oxygen at the temperatures under consideration. More plasticity is often associated with a scale which is more non-stoichiometric. It supports the prediction that the scale formed in air is more plastic which is associated with increased O-vacancy defects due to incorporation of nitrogen atoms.



The observation that the difference in weight gain in the initial stages between the two cases of oxidation, i.e., in air and in oxygen decreases with increasing temperature of oxidation may be attributed to a possible increase in the reactivity of nitrogen with niobium. The process of niobium reacting with nitrogen appears to be more favoured than the dissolution of N-atoms <sup>in</sup> zirconia scale with increasing temperature. If it so occurs, the excess vacancies created by substantial dissolution of nitrogen present in air will be decreased leading to a comparatively lower weight gain resulting in decrease of the difference in the weight gains, for the two cases with increasing temperature. This view of increased reactivity of nitrogen with niobium with increasing temperature may be supported by the work of Albrecht and Goede.<sup>43</sup> They observed that below 1000°C,  $Nb_2N$  and  $NbN$  were produced whereas at still higher temperatures the reaction produces only  $NbN$ . Niobium forms a number of different nitrides whereas zirconium forms only one nitride, viz.,  $ZrN$ . This may indicate that the reactivity of nitrogen is more for niobium than for zirconium. To this it may be added that Nb-N system is complex. A small addition of C and O, as suggested by Felten,<sup>70</sup> may lead to a number of new phases. This may be one reason why it was not possible to detect the presence of nitrides of niobium in x-ray analysis. Even if it is formed, its amount would have been very less for identification. It may be pointed out that Schönberg<sup>41</sup> and recently Guard et al.<sup>42</sup> found presence of five phases for  $NbN$  systems which perhaps

supports high reactivity of niobium with nitrogen.

Thus what has been said appears to account for decreasing difference in weight gain with increasing temperature of oxidation. However, such comparison is valid only for initial stages of oxidation. Due to added complications in the later stages no single explanation can be given.

### 3.6 Effect of History of the Samples:

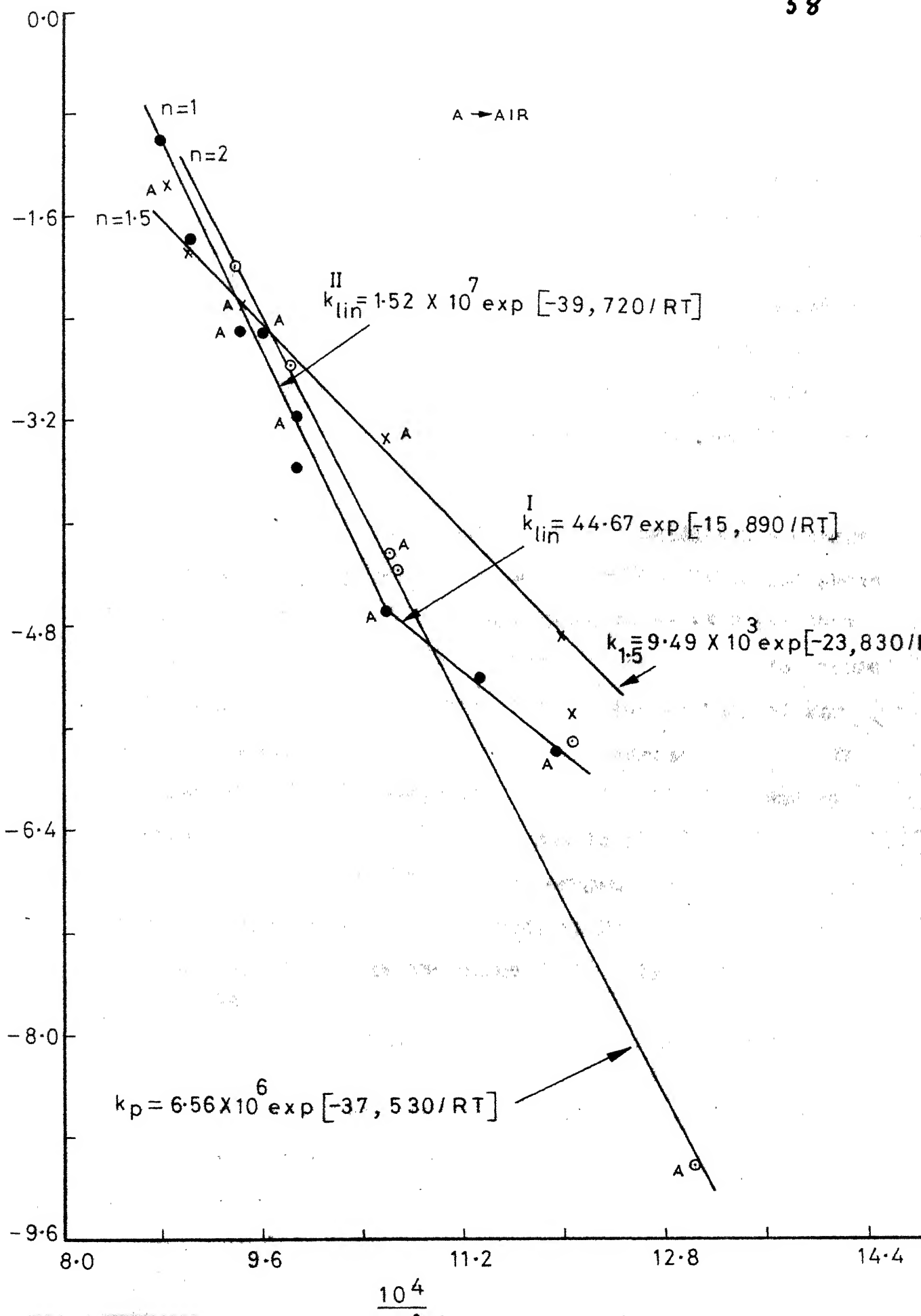
Annealed and unannealed samples were employed to observe effect of annealing on oxidation behaviour. Samples in category 2 were unannealed whereas those in category 3 were annealed at  $800^{\circ}\text{C}$  for 1 hr. under a pressure of  $10^{-6}$  mm.

Fig. 5 gives plot of the weight-gain curves for annealed samples, and Fig. 4 that for unannealed ones. It appears from the curves that weight gain is smaller for the annealed samples than that for the unannealed samples. It seems to be associated with the coarseness of the niobium-rich phase observed from metallographic observations, and will be taken in more details in 'general discussions'.

### 3.7 Activation Energies:

The Arrhenius plot for both the results in air and oxygen is given in Fig. 10. It is clear from the figure that the activation energy is same in both the cases. Thus one expects that reaction mechanism in both cases of reaction in air as well as in oxygen essentially remains the same.





The activation energy for parabolic oxidation has been calculated and is found to be 37.5 kcal/mole in the present case. This agrees well with the reported value of 36 kcal/mole in literature,<sup>6,16,18,71,72</sup> It may be concluded that in parabolic oxidation of Zr-2.5 wt. pct. Nb alloy the same mechanism of oxidation as for the case of pure zirconium operates, viz., diffusion of oxygen ions through O-vacancies in the oxide.

Fig. 10 indicates that for linear oxidation a change in activation energy occurs at around 670°C. Below and above 670°C, the activation energy, was found to be 15.9 and 39.7 kcal/mole respectively. It is difficult to account for these activation energies in the linear range due to lack of our knowledge about the processes occurring during reaction. In the lower temperature range the observed activation energy of 15.9 kcal/mole may probably be due to phase boundary reaction as the controlling step leading to oxygen dissolution. This value is close to activation energy of 20 kcal/mole for linear oxidation of niobium in the range where  $Q$  is independent of pressure.<sup>73</sup>

The other value of 39.7 kcal/mole corresponding to temperature above 670°C may be associated with the phase boundary reaction as controlling step after rupture of the initial oxide scale. The rupture of the scale occurs after certain stress is built up.

One more aspect may be mentioned here about the activation energies corresponding to linear kinetics. The mechanism for the linear law can be expected to obey that proposed by Ehrlich's model.<sup>74</sup> According to this, a gradual decrease in activation energy should be expected with increasing temperature. While such a temperature dependence has been observed with linear growth of  $Ta_2O_5$ , the present work does not reveal any such decrease in  $Q$  with temperature upto  $870^\circ C$ . However, it may be emphasized that the presence of niobium in the alloy may cause unpredictable changes, the interpretation of which can not be easily made.

The activation energies associated with other rate laws in this investigation corresponding to other  $n$  values given in Table 4 can not be easily related to processes occurring during the reaction because mechanisms for such processes are not well understood. The values of activation energies of oxidation for the alloy obeying non-parabolic rate laws are not available in literature, hence a comparison can not be made.

It may be pointed out here that the high activation energy shown in the literature for oxygen dissolution in zirconium metal, viz. around 51 kcal/mole suggests that weight gain due to O-solubility would be more and more significant with increasing temperature of oxidation.

## CHAPTER 4

### PHYSICAL FEATURES OF OXIDE FILMS AND METALLOGRAPHY

#### 4.1 Physical Features:

Table 6 shows some of the physical features of the oxide films observed on the alloy substrate.

Table 6

#### Physical Features of Oxidized Samples

Sample	Final colour of oxide surface	Relative degree of adherence of the oxide on substrate	Remarks
I	Surface near edge is white, interior is mottled	easily detachable	1. formation of white oxide on way. 2. smooth (no cracks) oxides surface 3. Sample not buckled
II	White oxide surface with slight black tinge		Smooth surface, sample not buckled
IV	Complete black surface	easily detachable	smooth surface, sample not buckled
V	Complete black surface	easily detachable	smooth surface, sample not buckled
VI	Periphery turned white, interior mottled	oxide on periphery more adherent than oxide in the interior of the sur-	smooth surface, sample not buckled

Table 6 contd,...

VII	Complete white surface	hard, adherent scale	smooth surface, sample not buckled, white oxide layer far more thicker than the inner black layer
XIII	mottled surface		
1	grey		smooth, surface, sample not buckled
2	Complete white		smooth surface, sample white layer far more thicker than the inner black
4	grey		smooth surface, sample not buckled white oxide formation on way
5	grey	black oxide layer more adherent than white layer	smooth surface, sample not buckled
6	All black surface		smooth surface, sample not buckled
7	mottled surface		smooth surface, sample not buckled, white oxide formation preferred on peripheral region.:
8	Black		smooth surface, sample not buckled, oxide layer formed is comparatively very thin
9	Complete white		smooth surface except periphery where some cracks appeared, sample not buckled
10	grey		
11	Complete white		smooth surface, sample not buckled
12	All-black		smooth surface, sample not buckled

Table 6 contd...

13	All white		surface not smooth (cracks visible), sample not buckled
14	All-white		Lot of surface cracks visible, sample buckled
15	White edges, interior grey		sample buckled
two			sample buckled, and turned brittle
three	All white	low adherence of the oxide	oxide appeared to flake off
four			sample buckled, but not turned brittle (remains elastic)
six	All-white		Sample elastically buckled
seven	Black		smooth surface, sample not buckled
eight	White near edges, interior on easier to black	<sup>interior</sup> black portion easier to descale	smooth surface, sample not buckled
nine	grey		sample elastically buckled
ten	white on edges, interior mottled		smooth surface, sample not buckled, coverage of the surface with white oxide approaching completion

Colour of the oxide:

The oxide film formed in the initial stages was black in colour. But if sufficient time was allowed depending on temperature of oxidation, formation of white oxide was obser-

grew with time and eventually covered the whole surface.

The photograph  $M_6$  for the oxidized Sample 7 indicates that formation of white (stoichiometric) zirconia scale started in general on the edges of the samples.

#### Adherence of the film:

During stripping the substrate from its oxide layer, 'relative' degree of adherence of the latter was carefully noted. The results are shown in Table 6. Observations on Sample IV and V which were oxidized at 396 and 494°C respectively suggest that the low temperature non-stoichiometric zirconium oxide (black in appearance) was easily detachable. When a layer of white oxide has been formed, the black oxide appears to be more adherent than the white oxide as observed for Sample eight which was oxidized at 746°C. Similar observation was made for Sample 5 which was oxidized at 690°C. Sample three which was oxidized at 834°C and formed white surface after oxidation showed spalling of the oxide. The oxide on periphery of the sample appeared to be in general more adherent than that in the interior. An adherent oxide on the periphery which was formed on the periphery of the Sample 1 is shown in Photograph  $M_{19}$ .

The varying degree of adherence of the oxide appears to bear a relation with its tendency to crack, thereby affecting the kinetics of oxidation. More adherence of the oxide observed on the periphery possibly leads to initiate the formation of white oxide.

#### 4.2 Macrographs:

Photographs  $M_1$ - $M_9$  show macrographs of some of the samples at a magnification between 10 and 15. These macrographs represent the following observations -

(a) Macrographs  $M_1$  and  $M_2$  show typical grains revealed of the etched samples prior to oxidation.

(b) Macrograph  $M_3$  indicates that where white oxide formation took place, a layer of inner black film beneath the white layer was observed by stripping a part of the substrate of the oxide.

(c) Macrograph  $M_4$  shows appearance of cracks over the oxide surface. Cracks were observed with a few of the oxidized samples. Cracks tended to concentrate on the edges.

(d) Macrograph  $M_7$  shows a specimen surface with completely black oxide. White oxide formation has not yet occurred. Micrograph  $M_5$  depicts the surface of a specimen completely covered with white oxide. Macrograph  $M_8$  represents the formation of mottled oxide on the surface.

(e) Macrograph  $M_6$  shows the first appearance of white oxide near edges of the samples.

(f) The surface of a specimen buckled after oxidation is shown in Macrograph  $M_9$ .

One may expect that if there is any preferential oxidation on the grain boundaries descaling the substrate may





$M_1$  (Sample 2)



$M_2$  (Sample 11)

$M_1, M_2$  - surface of the samples before oxidation showing typical grains



$M_3$  (Sample 2)



$M_4$  (Sample 9)

$M_3, M_4$  - surface of the samples after oxidation showing cracks on the oxide surface. Crack initiates to form on periphery.



M5  
(Sample 7)  
surface  
before  
oxidation



M6  
(Sample 7)  
surface  
after  
oxidation



M7  
(Sample 8)  
surface  
after  
oxidation



M8  
(Sample 6)  
surface  
after  
oxidation

M9  
(Sample 15)  
surface after  
oxidation,  
sample buckled



M5, M6 show grains less during oxidation  
M6 shows white oxide, forming first on the p  
Black and white oxide formed. M3, M7 and depict respectively a black and mottled, of the oxide.

reveal coarsening of the boundaries. A comparison of Macrographs of Sample 2 ( $M_1$  and  $M_3$ ) or of Sample #7 ( $M_5$  and  $M_6$ ), however, indicates that in the present investigation no such coarsening of the grain boundaries was revealed. In the present investigations, it may be concluded from these observations that the grain boundary reaction was insignificant.

The appearance of visible cracks on oxide surfaces with some of the oxidized samples might be a result of thermal cooling from temperature of oxidation. It is possible that the cracks may not be present at the temperature of oxidation during the oxidation reaction.

Observed buckling of some samples may be due to the difference in rate of oxidation on the surfaces exposed. According to Saur et al.<sup>75</sup>, differences in surface roughness may be responsible for differential oxidation rates. It was observed that the buckling of a specimen depended on the thickness of the sample, temperature and time of its oxidation. Generally the samples of thickness above 0.04 cm did not buckle.

Occurrence of buckling at the temperature of oxidation may lead to early appearance of cracks in the oxide which may subsequently change the oxidation kinetics. This would, however, also depend on plasticity of the oxide formed.

### 4.3 Micrographs:

#### 4.3.1 Micrographs with Ordinary Light:

Photographs  $M_{10}-M_{35}$  show micrographs of oxidized and unoxidized samples under a magnification of 300. Sample numbers to which these micrographs refer are mentioned against them. These micrographs were taken using ordinary light. Polarized light was also used with some samples. Pictures  $M_{36}-M_{38}$  are the photographs of the samples with polarised light and will be discussed in section 4.3.2.

The micrographs taken in ordinary light represent the following observations:

(a) Micrographs of Sample four shown in  $M_{20}$  shows the typical niobium-rich second phase precipitated in a Widmanns-tatten pattern in the matrix.

(b) The photomicrograph of an unannealed sample is given in  $M_{21}$  whereas those of the annealed samples are given in  $M_{22}-M_{27}$ . It appears that coarsening of the second phase has occurred after the annealing treatment.

(c)  $M_{10}-M_{18}$  show micrographs of the substrate after removal of oxide layers.

Micrographs  $M_{10}-M_{13}$  for Category I show that coarsening of the second phase increased with increasing temperature of oxidation.  $M_{14}-M_{16}$  show the same result for Category II, and  $M_{17}-M_{18}$  show it for Category III.

(d) Coarsening of the second phase increased in going from Category I to Category III in general as seen from Micrographs  $M_{10}-M_{18}$ .

Cat. I →  
showing  
various  
Nb-rich  
phase  
with  
increasing  
temp. of  
oxidation



M10  
(Sample V)



M11  
(Sample VIII)



M12  
(Sample I)



M13  
(Sample VII)

Cat. II →



M14  
(Sample 10)



M15  
(Sample 9)



M16  
(Sample 14)

Cat. III →



M17  
(Sample seven)



M18  
(Sample four)

M10 - M18 show substrates after oxidation



M19  
(Sample 1)  
showing  
adherent  
oxide  
on  
periphery  
of  
the sample

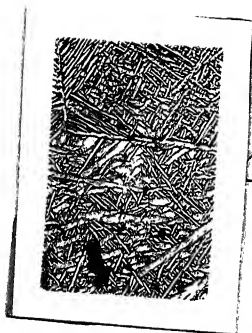
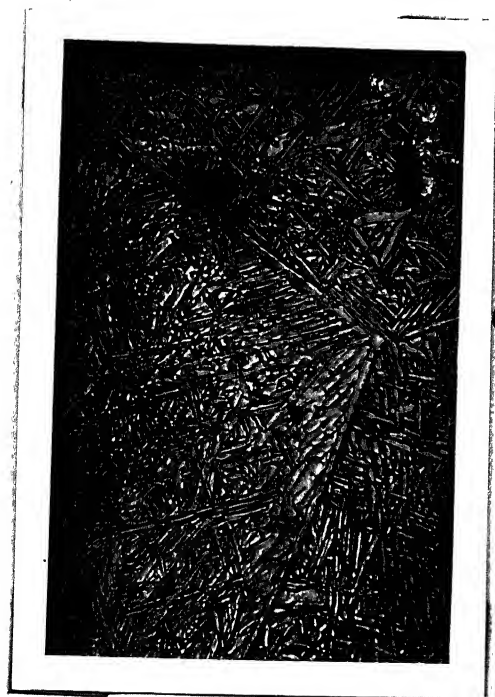
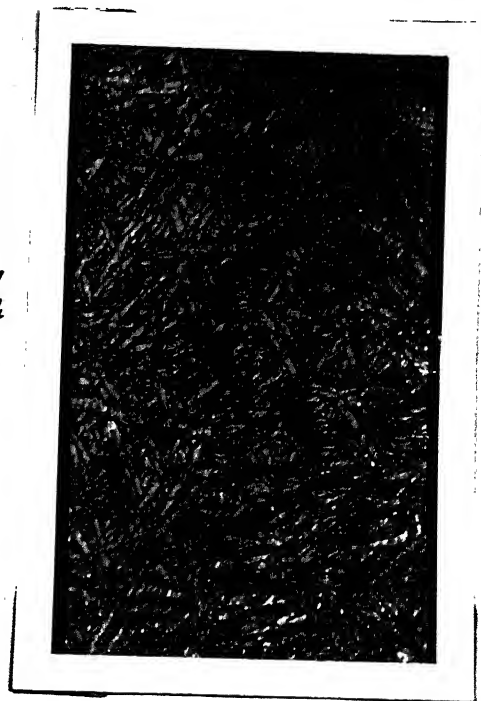
M19

M20  
(Sample four)  
showing  
Widmanstätten  
structure

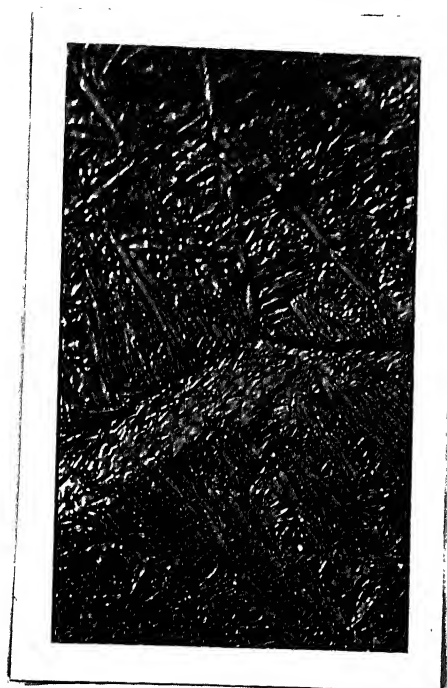
M20



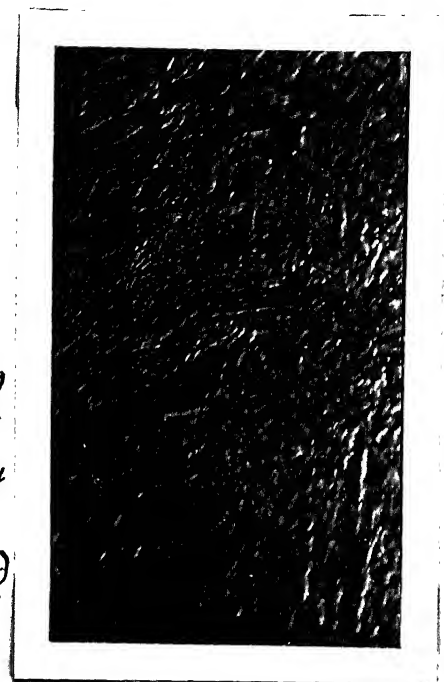
M<sub>21</sub>: as-received alloy surface before  
 M<sub>22</sub>, M<sub>24</sub>, M<sub>26</sub>: annealed sample  
 surfaces before oxidation  
 M<sub>23</sub>, M<sub>25</sub>, M<sub>27</sub>: surfaces of the  
 samples after their oxidation

M<sub>21</sub> (Sample 3)M<sub>22</sub>  
(Sample six)M<sub>23</sub>  
(Sample six)M<sub>24</sub>  
(Sample nine)M<sub>25</sub>  
(Sample nine)M<sub>26</sub>  
(Sample seven)M<sub>27</sub>  
(Sample seven)

M<sub>21</sub>: as-received alloy surface (before oxidation)  
 M<sub>22</sub>, M<sub>24</sub>, M<sub>26</sub>: annealed sample surfaces before oxidation  
 M<sub>23</sub>, M<sub>25</sub>, M<sub>27</sub>: surfaces of the annealed samples after oxidation  
 Pictures showing effect of annealing and Oxidation treatment on coarsening of Nb -



M28  
Sample  
9  
(interior  
of  
the  
specimen)



M29  
Sample  
9  
(periphery  
of  
the  
specimen)

M28 and M29 show structure of the substrate after oxidation. The oxidation treatment does not appear to cause any detectable difference in microstructure on the two regions of the substrate.



M30 (Sample 13)  
decalcified substrate  
in focus



M31 (Sample 6)  
decalcified substrate  
in focus



M32 (Sample 12)  
decalcified substrate in  
focus



M33 (Sample 13)  
oxide surface in focus



M34 (Sample 6)  
oxide surface in focus



M35 (Sample 12)  
oxide surface in focus

M30 - M35 show regions on the specimen surfaces consisting of oxide surface and decalcified substrate. The interface can be studied with the help of such micrographs.



(e)  $M_{22}$ ,  $M_{24}$  and  $M_{26}$  are micrographs of the three samples before oxidation and  $M_{23}$ - $M_{25}$  and  $M_{27}$  are those of the same samples respectively after oxidation with oxide removed. From this, it is observed that coarsening occurred after oxidation.

(f)  $M_{28}$  shows micrographs of Sample A 9, oxidized and descaled, over an area lying in the interior of the surface.  $M_{29}$  shows micrograph of the same sample after similar treatment near its periphery. A comparison of the two micrographs shows that there has been essentially no difference in surface structure of the two regions of the same surface after oxidation.

(g) Micrographs  $M_{30}$ - $M_{35}$  show the regions on the junction of oxide surface and descaled surface. Bare descaled surface has been shown in focus for three samples in  $M_{30}$ - $M_{32}$  whereas  $M_{33}$ - $M_{35}$  show the same regions for the corresponding samples with oxide scale in focus. These micrographs were taken in order to study the descaled surface in relation with the surface of oxide on the junction. However no significant information could be deduced from these observations.

Appearance of coarsening of niobium-rich phase suggests that coarsening is dependent on temperature as well as time of oxidation. Annealing produces coarser structure than what it was for the unannealed specimens. The degree of coarsening appears to bear relation with subsequent oxidation of the alloy.



A decrease in weight gain observed for the annealed samples thus seems to result from coarser second phase for these samples. This aspect will be further <sup>taken</sup> in 'general discussion'.

As mentioned under (f) above, there was essentially no difference observed in the structure of the substrate at the periphery and in the interior of it. The photograph of the substrate does not reveal that there exists a difference between oxidation behaviour near the sample edges and in the interior of the surface.

#### 4.3.2 Micrographs with Polarized Light:

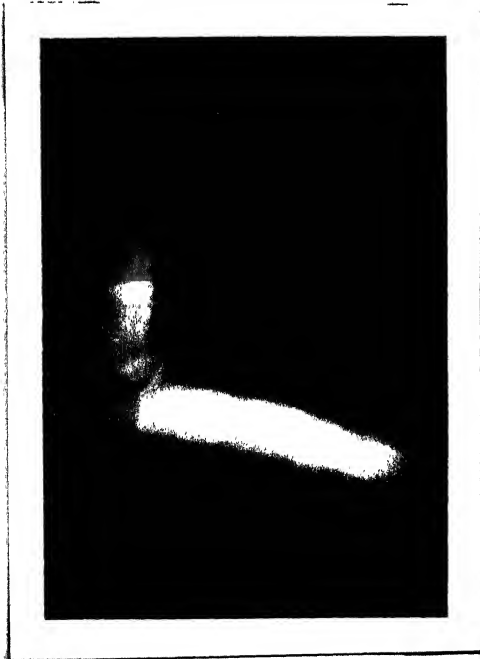
Pictures  $M_{36}$ - $M_{38}$  were taken with polarized light at a magnification of 400 in order to detect a possible existence of oxide layers formed due to transition cycles.  $M_{36}$  and  $M_{37}$  show oxide layers. The layers were not observed with ordinary light ( $M_{38}$ ). The attempts to correlate the number of oxide layers with the number of transition cycles failed. Distinct layers amenable to easy counting could not be observed. It is not unreasonable to think that, in general, some of the layers could fuse together at the temperature of oxidation as well as during subsequent cooling.

M36  
(Sample  
VII)



M36 and M37 show micrographs taken with polarized light. The pictures depict the occurrence of oxide layers.

M37  
(Sample  
2)



M38 shows a micrograph taken with unpolarized light. Occurrence of oxide layers in it is not observed.

M38  
(Sample 2)  
same region  
as in M37,  
photographed



Table 7

Calculated d-Values from Powder Patterns

target - copper, filter - nickel

Sample	d cal (Å)	Relative intensity (visual esti- mate)  (I/I <sub>1</sub> )	d cal (Å)	Relative intensity (visual estimate)  I/I <sub>1</sub>
11 (white frac- tion of oxide)	3.674 2.847 2.541 2.324 2.034 1.859 1.703 1.543 1.425 1.270	30 90 40 5 10 40 30 30 30 3	3.159 2.629 2.369 2.200 1.999 1.819 1.659 1.484 1.324	100 75 5 75 10 75 75 30 30
11 (black frac- tion)	3.689 2.838 2.595 1.851 1.697 1.548	70 90 40 20 20 5	3.162 2.635 2.213 1.815 1.660 1.433	100 70 40 70 65 5
13 (white frac- tion)	3.648 2.836 2.321 2.008 1.694 1.598 1.479 1.369 1.265 1.109 0.939 0.884 0.842 0.806	90 98 60 70 70 68 70 30 65 65 50 70 50 70	3.143 2.599 2.189 1.808 1.656 1.541 1.422 1.322 1.161 1.034 0.906 0.864 0.818	100 90 85 95 85 85 70 65 65 70 48 50 60

Table 7 contd...

Sample	d	I/I <sub>1</sub>	d	I/I <sub>1</sub>
13	3.996	80	3.678	80
(black	3.154	100	2.831	87
fraction)	2.633	82	2.198	82
	1.983	95	1.812	90
	1.640	75	1.533	75
	1.414	80	0.952	46
	0.863	85	0.841	85
14	3.610	77	3.137	100
	2.840	98	2.589	80
	2.298	40	2.173	80
	1.999	98	1.807	92
	1.652	85	1.537	85
	1.475	75	1.417	85
	1.324	60	1.273	50
	1.030	55	0.998	55
	0.934	60	0.886	65
	0.864	65	0.844	65
	0.808	50		
three	5.183	50	5.693	60
(white	3.148	100	2.842	100
fraction)	2.631	60	2.541	45
	2.338	2	2.213	60
	2.026	5	1.850	50
	1.819	75	1.699	50
	1.661	50	1.607	5
	1.585	5	1.547	50
	1.479	50	1.420	50
three	3.663	35	3.162	100
(black	2.838	95	2.629	55
fraction)	2.473	85	2.213	25
	2.023	10	1.853	35
	1.822	65	1.708	35
	1.664	50	1.545	35
	1.480	30	1.424	25
I	3.612	65	3.148	100
	2.845	90	2.622	80
	2.327	80	2.004	100
	1.754	75	1.661	75
	1.425	60	1.364	75
	0.863	80	0.838	80

Table 7 contd...

Sample	d	I/I <sub>1</sub>	d	I/I <sub>1</sub>
II	3.943	60	3.641	60
	3.137	90	2.818	90
	2.614	75	2.427	60
	2.209	75	1.988	100
	1.816	85	1.736	60
	1.649	75	1.589	40
	1.541	45	1.479	45
	1.420	80	0.863	80
	0.838	80		
VII (white)	3.659	60	3.493	70
	3.165	100	2.856	95
	2.626	70	2.539	60
	2.217	60	2.010	25
	1.855	25	1.819	50
	1.702	25	1.657	50
	1.547	15	1.491	5
	1.431	5		
1 (black)	3.626	65	3.165	100
	2.831	96	2.607	85
	2.467	90	2.210	50
	2.004	50	1.814	65
2	3.666	40	3.162	100
	2.834	90	2.622	40
	2.450	50	2.327	5
	2.203	30	1.843	5
	1.809	30	1.689	5
	1.654	5	1.552	5
	1.426	30		

Nb  
 $\text{Nb}_2\text{O}_5$  as one of its constituents. NbO was found to be absent in it. Apart from stoichiometric  $\text{ZrO}_2$ , white portion was found to contain NbO with no trace of  $\text{Nb}_2\text{O}_5$  in it. Thus both fractions contained  $\text{ZrO}_2$  (Baddeleyite structure) as a major constituent of the oxide phase.

Sample obtained from DTA measurements did not reveal lines corresponding to  $\text{Nb}_2\text{O}_5$  in its X-ray pattern. Presence of NbO lines with predominant lines corresponding to  $\text{ZrO}_2$  (Baddeleyite) was, however, observed.

The X-ray pattern result for unoxidized, pure alloy powder given in Table 8 indicates the lines corresponding to alpha - zirconium. No line corresponded to pattern of niobium.

The observations indicate that NbO is more favoured oxide to be formed with increasing temperature rather than  $\text{Nb}_2\text{O}_5$ . Failure to detect lines of  $\text{Nb}_2\text{O}_5$  from DTA powder sample, corresponding to oxidation upto  $1260^\circ\text{C}$ , appears to suggest that the tendency of the <sup>oxide</sup> to exist in  $\text{Nb}_2\text{O}_5$  form decreases with increasing temperature. It is known, however, that during oxidation of pure niobium, the oxide  $\text{Nb}_2\text{O}_5$  is a stable phase around the temperature mentioned. It may be assumed therefore that the disappearance of  $\text{Nb}_2\text{O}_5$  in the present case may be due to formation of some complex oxides at high temperatures. Quarrel<sup>76</sup> has also suggested for the case of niobium alloys that in presence of other elements niobium may form oxides other than  $\text{Nb}_2\text{O}_5$ .

The presence of  $\text{NbO}_2$  was not observed with any of the samples. According to Brauer<sup>77</sup> NbO is very stable and does not decompose into Nb and  $\text{NbO}_2$ . However he concluded from his observations that NbO in nitrogen atmosphere can react with nitrogen to produce  $\text{NbO}_2$  according to reaction  $2\text{NbO} + \frac{1}{2}\text{N}_2 -$

Table 8

## Identified Oxidation Products from Powder Patterns

Sample	Temperature of oxidation (°C)	Colour of powder sample	Possible products
I	557	grey	$ZrO_2$ , $Nb_2O_5$
II	565	grey	$ZrO_2$ , $Nb_2O_5$
VII	670	white	$ZrO_2$ ,
1	670	black	$ZrO_2$ , $Nb_2O_5$
2	770	black	$ZrO_2$ , $Nb_2O_5$
9	788	white	$ZrO_2$
11	746	white	$ZrO_2$ , NbO
13	860	white	$ZrO_2$ , NbO, $Nb_2N$
1		black	$ZrO_2$ , $Nb_2O_5$ , $Nb_2N$
14	852		$ZrO_2$ , NbO, $Nb_2N$
three	834	white	$ZrO_2$
		black	$ZrO_2$ , $Nb_2O_5$
six	738		$ZrO_2$
pure alloy			$\alpha$ Zr
DTA oxide	upto 1260		$ZrO_2$ , NbO, $Nb_2N$

As expected, the predominance of  $ZrO_2$  in all the fractions of the oxide layer investigated in this work was observed. Any product of interaction of niobium with zirconia scale was not detected due to non-availability of X-ray data for such

complex oxides. Greenbaur and Harper<sup>55</sup> while investigating the effect of dissolution of niobium in zirconia oxide did not observe any change in the structure of the oxide.

The presence of  $\text{Nb}_2\text{O}_5$  and  $\text{NbO}$  oxides in the oxide layers may be associated with various changes occurring during the kinetics. Since  $\text{Nb}_2\text{O}_5$  has high volume ratio, its formation may result in crack formation and subsequent increase in oxidation rate. Intermittent occurrence of such cracks may explain the appearance of transition cycles in the weight gain curves.

The change in stability of  $\text{Nb}_2\text{O}_5$  with temperature as mentioned earlier may therefore account for some of the temperature dependent oxidation behaviour observed in present investigation. This aspect will further be taken in 'general discussion'.

## 5.2 Differential Thermal Analysis:

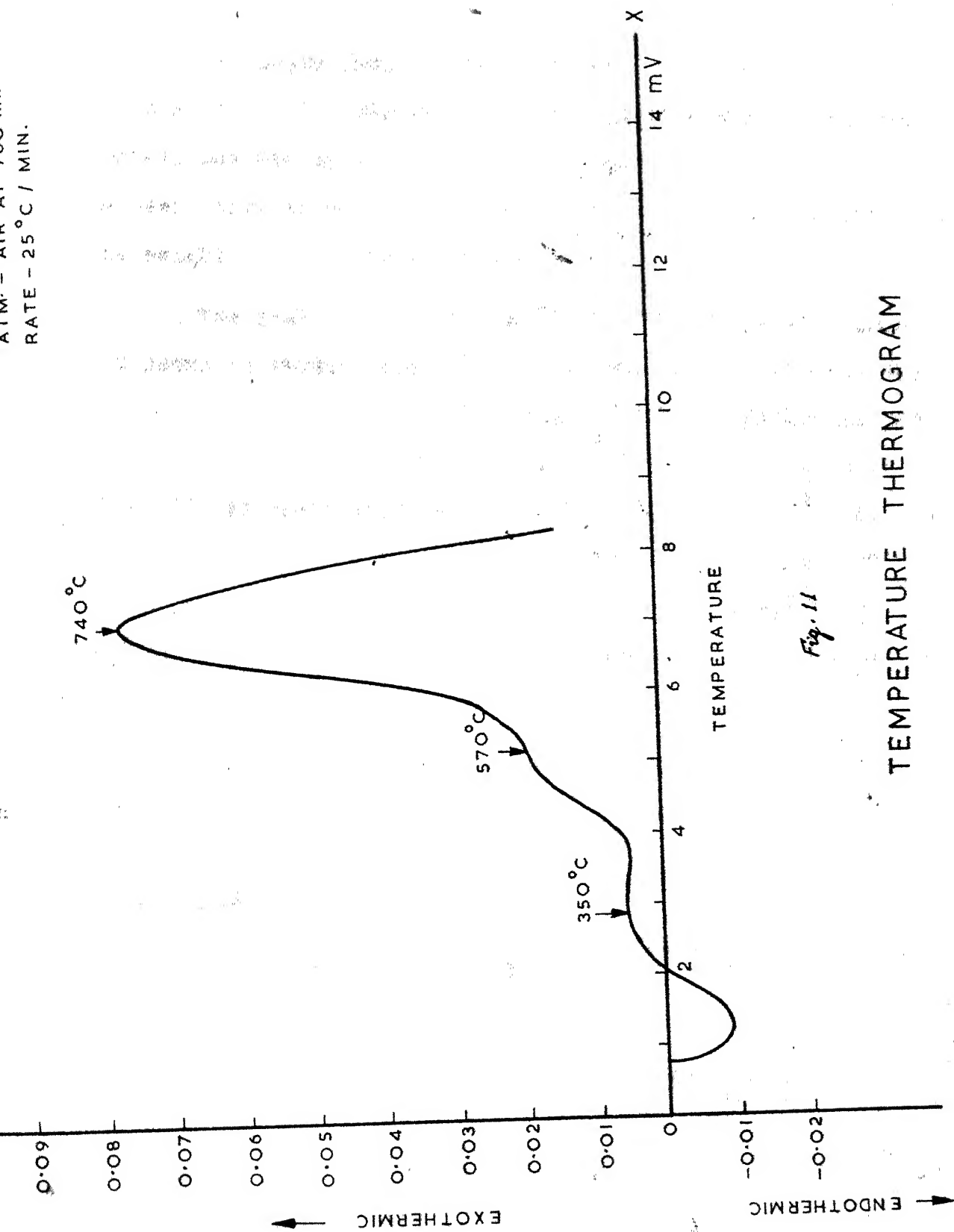
The du Pont 900 Differential Thermal Analyser was employed to record a temperature thermogram of a powder sample of the alloy.

Maximum temperature reached during the analysis was around  $1260^\circ\text{C}$ . Fig. 11 shows a meaningful portion of the thermogram. Conditions of the experiment are listed in the legend given in this figure.

It is seen from Fig. 11 that three prominent peaks were observed at temperatures  $350^\circ\text{C}$ ,  $570^\circ\text{C}$  and  $740^\circ\text{C}$ .



ATM - 100  
RATE - 25°C / MIN.



The peaks found at 350 and 570°C appear to correspond to some oxidation states. However, X-ray analysis did not reveal any new oxide formation at these temperatures. It appears that these temperatures correspond to abrupt increase in weight gain during oxidation.

The peak observed at 740°C was relatively very large. It seems to result from ignition of the alloy powder at this temperature. Literature reveals that zirconium powder is pyrophoric,<sup>78</sup> and for that matter, it is susceptible to rapid ignition if conditions are favoured. The temperature of ignition depends on particle size of the powder. A particle size as low as 3.3 micron can self ignite in air.<sup>78</sup>

A discontinuity in the curve (perhaps a very feeble peak) was observed at 1215°C (not shown in Fig. 11) which may be associated with presence of niobium in the powder. Klopp, Sims and Jaffer<sup>45</sup> reported that at 1400°C the heat of reaction was sufficient to melt the niobium metal. Work is needed to discover the <sup>cause</sup> ~~course~~.

No more meaning could be assigned to this analysis.

## CHAPTER 6

### DIFFRACTOGRAMS

Diffractiongram of the alloy substrate after descaling the surface oxide was taken for one of the samples, viz., Sample seven. Table 9 gives  $2\theta$  values and relative intensity of the peaks observed in this case. It also included the calculated  $d$  values from the diffractiongram data. A diffractiongram was also taken on the unoxidized alloy sample.

It is observed from Table 9 that completely descaled surface of Sample seven showed peaks only due to alpha-zirconium. The peaks observed were as sharp as those obtained for the case of unoxidized alloy. It suggests that the alloy did not pick up appreciable amount of oxygen as the temperature of oxidation was low. It is in accord with high activation energy of O-dissolution in zirconium metal.

Table 9  
Diffractiongram Results for Sample Seven

$2\theta$	$d_{cal}$	Relative intensity ( $I/I_1$ )
32.00	2.797	10
34.80	2.578	15
36.50	2.462	100
68.40	1.371	9
117.40	0.902	2

Diffraction patterns were also taken on those samples which formed oxide insufficient for making powder to be employed in the Debye-Scherrer method. This involved samples which were oxidized at around  $500^{\circ}\text{C}$  or lower. Fig. 12 shows a part of the diffraction pattern observed for Sample V which was oxidized at  $494^{\circ}\text{C}$ .

A study of the diffraction patterns such as one shown for Sample V in Fig. 12 led to a conclusion that the specimens oxidized at low temperatures, around  $500^{\circ}\text{C}$  or below, showed presence of alpha-zirconium and  $\text{ZrO}_2$ , although no sharp peak of the oxide was detected. Before taking diffraction pattern, half of the surface of Sample V was stripped of the scale so that both the oxide as well as substrate could be exposed to X-ray beam during recording diffraction pattern. Due to this alpha-zirconium peaks were also observed in the diffraction pattern of Sample V. Peaks corresponding to  $\text{Nb}_2\text{O}_5$  or any other oxide of niobium was not detected. This is supported by the work of Brauer<sup>79</sup> who did not detect sharp lines corresponding to  $\text{Nb}_2\text{O}_5$  during oxidation of niobium below  $500^{\circ}\text{C}$ . He assumed that amorphous films formed. In the present investigation also it appears that formation of amorphous films of  $\text{Nb}_2\text{O}_5$  occurred at low temperatures. Due to its low amount in the oxide layer and its amorphous nature, the presence of  $\text{Nb}_2\text{O}_5$  in the film was difficult to determine by diffraction patterns.

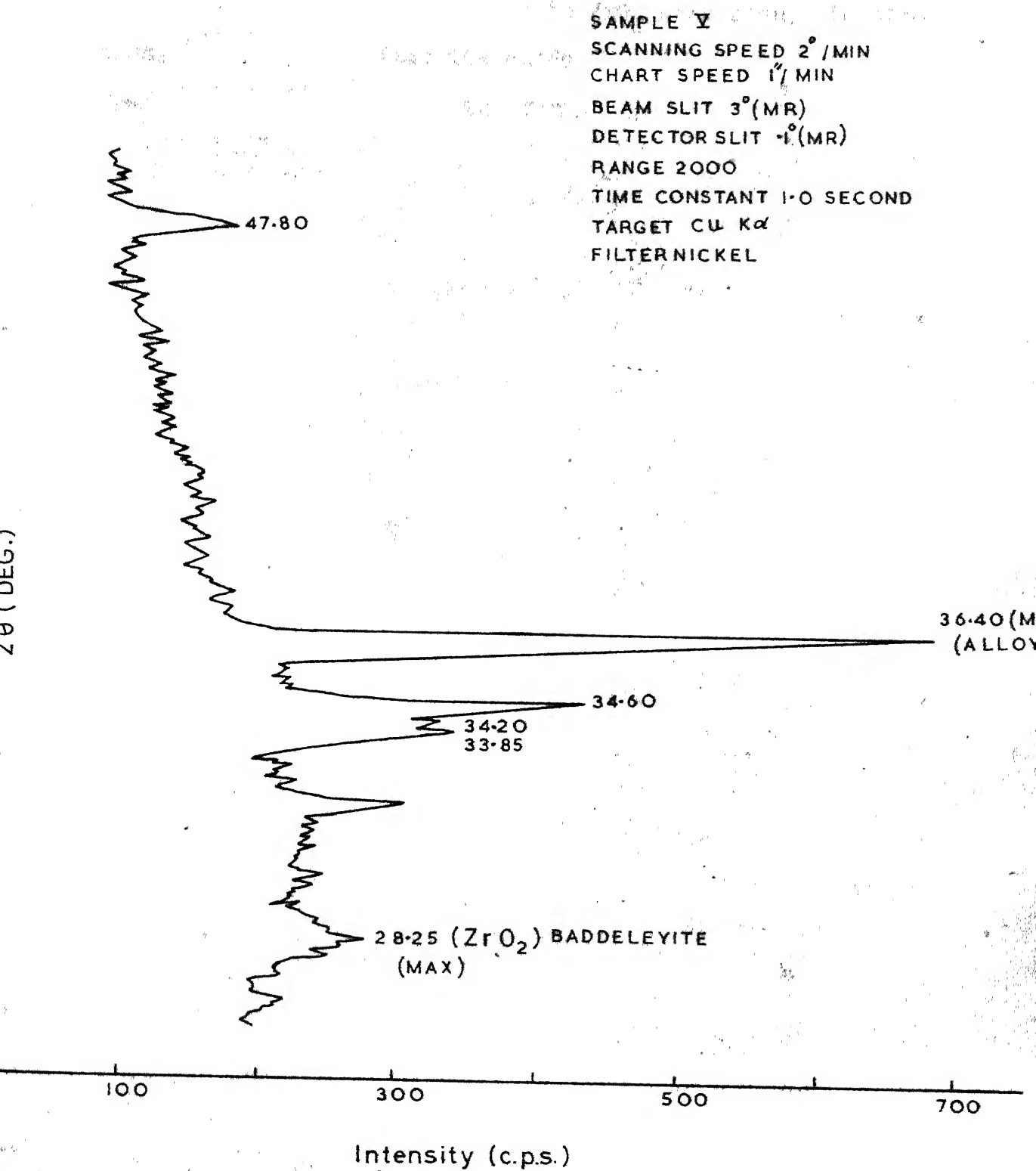


Fig. 12 - A Part of the Diffractogram Taken on Sample V, Oxidized at  $494^{\circ}\text{C}$ .

Weak peaks corresponding to  $\text{ZrO}_2$  were always identified. This suggests that the oxide is still in transition from amorphous to crystalline form.

## CHAPTER 7

### MICROHARDNESS

Knoop hardness measurements were taken for all the samples employing 1 Kg indentation load. The result is expressed as the Knoop Hardness Number. The Knoop indenter was pyramidal in form giving a diamond-shaped (rhomboidal) indentation of which the diagonals had an approximate relation of 7 to 1. The Knoop Hardness Number relates the applied load in Kg to the unrecovered (approximate) projected area in sq. mm. The hardness number corresponding to a measured length 'l' (length of longitudinal dimension of indentation) for a load of 1 kg was determined from a table supplied with the hardness tester.

The depth of indentation was about  $1/30$  the length of longitudinal diagonal.

Data for microhardness are given in Table 10 - 11 for some of the samples. Table 10 gives the values for unoxidized specimens in annealed and unannealed conditions. Table 11 gives the same for oxidized samples.

Table 10 shows that the hardness of the unoxidized samples decreased from a value of about 252 to a value of about 226 as a result of annealing treatment at  $800^{\circ}\text{C}$  for 1 hr. in  $10^{-6}$  mm Hg pressure.

Table 10

Hardness Values ( $KHN_{1kg}$ ) for Unoxidized Specimens

Unannealed <sup>1</sup>			Annealed <sup>2</sup>		
Length of indenta- tion 'l' (mm)	Average length of inden- tation (mm)	Average Hard- ness 'H'	Length of indenta- tion 'l' (mm)	Average length of indenta- tion (mm)	Average hardness
0.2375			0.2536		
0.2375	0.2375	252	0.2541	0.2509	226
			0.2451		

<sup>1</sup> measured on Sample 3<sup>2</sup> measured on Sample five and eleven

Table 11 gives hardness values taken on the oxide surface as well as on the stripped substrate. The hardness values of the substrate increased in general from those observed before oxidation as expected. However, this increase appears to be very small. The data thus led to conclude that oxygen penetrated only to a small layer of the substrate. After polishing the substrate surface down to about 0.5 mm the measured hardness returned to normal values obtained before oxidation.

From these data it is difficult to calculate the diffusion coefficient of oxygen in the alloy. The small penetration of the gas in the alloy for the present case also explains



Table 11

Hardness Values (KHN<sub>1</sub> kg) for Oxidized Samples

Category	Sample	Temperature of oxidation (°C) (increasing order for each category)	Average hardness measured on	
			descaled surface	Oxide surface
I	IV	396	279	279
	V	494	249	279
	VI	550	237	19
	VII	670	251	249
II	12	563	253	302
	7	672	243	15
	10	738	247	470
	9	788	247	229
	13	860	253	25
III	seven	595	239	
	eight	746	247	
	three	834	243	218

why the hardness values measured on the substrate do not reflect any detectable dependence on temperature of oxidation.

The observations showed that the hardness values at black oxide were as high as 470 for Sample 10. The hardness measured on white oxide surface showed an appreciable decrease.

The hardness measurements on the white oxide showed cracks around the indentations whereas those on the black oxide did not show cracks. It may be attributed to the loss of plasticity associated with formation of white oxide. The hardness values measured on white oxide were as low as 25 in case of Sample 13. It may be noted that Douglass<sup>20</sup> from his study on plasticity of zirconia concluded on the basis of smoothness of the indentations that calcia stabilized cubic zirconia was more plastic than monoclinic form.

The plasticity of the oxide bears relation with its protective property. A well plastic scale may stand minute dimensional changes which may occur due to thermal stresses set up in the oxide without tearing itself and thereby preserving its protective property. In case of insufficient plastic scale, the stresses generated in the oxide may lead to rupturing of the scale which will enhance the oxidation.

The hardness values measured on white oxide surface were not consistent. This observation is associated with cracking of the white oxide under the load of the indenter due to its brittle nature.

The hardness measurements taken around the black, non-stoichiometric zirconia surface of the oxide exposed as a result of gradient polishing on the junction between the oxide surface and descaled substrate showed that the hardness values increase from the bare part of the surface to the oxide. It

reflects increase in hardness with increasing concentration of oxygen in the metal.

Information obtained from hardness values for samples oxidized in air was more or less the same as in the case of oxidation in pure oxygen.

## CHAPTER 8

### GENERAL DISCUSSIONS

It is seen that transition cycles appear in the weight gain curves (Fig. 3-5). The oxidation rate may be enhanced with the formation of stoichiometric, porous,  $ZrO_2$  leading to a breakaway. However, a number of transition cycles observed can not be explained on the basis of enhanced oxidation accompanying the formation of stoichiometric, porous  $ZrO_2$  scale. It appears to be associated with the formation of oxides of niobium. The exceptionally high volume ratio of  $Nb_2O_5$  may lead to crack formation in the initial protective oxide and associated rapid rate of oxidation. However the subsequent reaction would again form protective oxide layer until rupturing of the protective scale again occurs by the same process bringing about onset of another cycle. This process seems to repeat and the corresponding number of cycles are observed in the weight gain curves.

At high temperatures, possibly a decrease in stability of  $Nb_2O_5$  in the scale may thus be expected to bring about less number of cycles as evidenced from the curves.

The enhanced oxidation rate at temperatures above  $700^\circ C$  may be due to formation of  $NbO$  oxide and lower stability of  $NbO_2$  and  $Nb_2O_5$  oxides in the scale. It was found by

Kofstad et al.<sup>80</sup> that  $\text{NbO}$  is less protective than  $\text{NbO}_2$  as the former formed on an inclined plane to the specimen surface.

The intermittent crack formation associated with high volume ratio of  $\text{Nb}_2\text{O}_5$  may cause transition cycles. It is expected that a coarser niobium-rich phase obtained after annealing of the samples (category III) may lead to improved corrosion resistance. For example, comparing the weight gain values for elapsed oxidation time of 20 minutes, it may be seen that Sample ten ( $611^\circ\text{C}$ ), six ( $738^\circ\text{C}$ ) and nine ( $742^\circ\text{C}$ ) show weight gain obviously less than  $1 \text{ mg/cm}^2$  (see Fig. 5) whereas gain in weight for Samples 11 ( $746^\circ\text{C}$ ), 2 ( $770^\circ\text{C}$ ) and 10 ( $738^\circ\text{C}$ ) is higher than  $1 \text{ mg/cm}^2$ . It suggests that annealing leads to improvement in corrosion resistance of Zr - 2.5 wt. pct. Nb alloy samples.

In view of fair stability of  $\text{Nb}_2\text{O}_5$  in case of oxidation of pure niobium at high temperatures and its less stability with increasing temperature in the presence case, it is possible that it may form some complex oxide with  $\text{ZrO}_2$ . The volume ratio and thermal expansion properties of the complex oxide would be altogether different. This may improve the oxidation resistance and cause decrease in transition cycles. It may be cited in this respect that Mayo and coworkers<sup>81</sup> have shown that improved oxidation resistance of Nb-Cr (35 - 50 pct.) alloy is attributed to the formation of a chromium niobate ( $\text{Cr NbO}_4$ ) complex. In a recent investigation on oxidation

study of zirconium-niobium alloy (1-20 wt. pct. Nb) in carbon dioxide atmosphere, Guerlet and Lehr<sup>51</sup> observed the formation of a complex oxide  $6 \text{ZrO}_2 \cdot \text{Nb}_2\text{O}_5$ . They pointed out that the tendency of formation of this complex increased with increase in temperature as well as with increase in niobium - content of the alloy. According to them the decrease in oxidation rate at  $900^\circ\text{C}$  in comparison to the rate at  $750^\circ\text{C}$  might be due to the formation of this complex.

It is observed that the occurrence of a transition cycle is delayed with increasing time. It is reasonable to think that  $\text{Nb}_2\text{O}_5$  causes cracking in the oxide as soon as  $\text{Nb}_2\text{O}_5$  film achieves a critical thickness. As the oxidation of the alloy proceeds, the time required to build up the critical thickness of the oxide ( $\text{Nb}_2\text{O}_5$ ) also increases. This may cause the observed delay.

Apart from high volume ratio of  $\text{Nb}_2\text{O}_5$ , the formation of stoichiometric, non-protective oxide layer may also be considered to cause change in the initial kinetics. The black and white fraction of the oxide did not show any difference in the structure of their  $\text{ZrO}_2$  content by X-ray observations (both showed Baddeleyite structure). However, it is generally known that black oxide is non-stoichiometric and protective whereas white fraction is stoichiometric and non-protective. Thus formation of white oxide is generally accompanied with enhanced rate of oxidation.

Stress concentration build-up in the oxide may also be responsible for the rapid rate of oxidation. The oxide rupture and resulting loss of its protective behaviour caused by stress generated in the oxide may at high temperature be completely counteracted by plastic flow and sintering in the scale.

Cox<sup>82</sup> proposed for the case of oxidation of pure zirconium that cracks might appear at grain boundaries due to stress concentration. A microscopic study (at magnification of 600) of the oxidized specimen was done but no local concentration of cracks was detected at or the grain boundary. This observation is not surprising in view of our little knowledge about the cause of transition. During the course of present investigation, Cox<sup>83</sup> reported the presence of cracks of the size 10-15 Å in the oxidation product of Zr-2.5 wt. pct. Nb from electron microscopic study. He attributed the occurrence of breakaway in the kinetics to the presence of these small cracks. The small cracks were thought to <sup>be</sup> generated by an oxide recrystallisation process. The occurrence of transition cycles was observed by him. He predicted this behaviour possibly due to large size cracks resulting from thermal cycling.

The increase in oxidation rate may also be expected as a result of preferential oxidation around inhomogeneities



in the oxide leading to crack formation due to stress concentration thus building up locally.<sup>84,85</sup> The effect could be more when the inhomogeneities are wide apart. In the present work, where the inhomogeneities (taken to be niobium-rich regions) are very uniformly distributed, this effect may be expected to be small. This effect may be insignificant in causing transition due to the important role played by high volume ratio of  $\text{Nb}_2\text{O}_5$ .

Cox and Johnston<sup>86</sup> observed rapid rate of oxidation just after transition to break away in the case of oxidation of pure niobium. Subsequently it becomes steady at linear. Kofstad<sup>85</sup> has suggested that the more rapid oxidation at the start of breakaway may possibly reflect a rapid nucleation and growth of  $\text{Nb}_2\text{O}_5$  (which is porous and offers no or little resistance to oxidation) on the surface, and attainment of a steady state process during the later stages. Thus the lower value of  $n$  ( $< 1$ ) obtained in the present work may be due to such nucleation and growth of the oxide.

The trend in variation of hardness values of the oxidized samples also bears relation to the kinetics. Hardness measured on the periphery was slightly higher than in the interior (hardness values on periphery were measured within 0.19 mm from the edge). It indicates edge effect in accord with the observed strong adherence of the oxide in peripheral region. Strong adherence reflects stress concentration which



may result in subsequent rupturing of the oxide on the edges. This edge effect in hardness measurements may be associated with early appearance of white oxide along edges of the specimen. This leads to decrease in oxidation resistance.

## CHAPTER 9

### NEED OF FUTURE WORK

Need of suitable models to explain low temperature oxidation behaviour (presumably where logarithmic law holds), and transition to linear and other kinetics at elevated temperatures, is not confined only to the present metals. Processes occurring during reaction at low temperature are in general the least understood as well as the field remains largely unexplored. There is no suitable mechanism proposed which can explain the linear oxidation.

Notwithstanding, there is need to further explore the above mentioned fields to arrive at a model which can satisfactorily explain with the mechanism proposed the observed oxidation behaviour. In particular, for the alloy used in the present work, future investigations are needed along the following lines.

(1) The exact nature of the defect structure of  $\text{ZrO}_2$ , the transport number of electrons, anions and cations are not known. There knowledge is necessary to understand the associated mechanism. It is generally assumed that the oxide growth is governed by oxygen diffusion. However, we should also consider the electrical characteristics of near-stoichiometric  $\text{ZrO}_2$  and

the transport number of ions and electrons, and thus whether migration of electrons through part of the scale is a rate-limiting factor. It is worthwhile to note in this respect that Bradhurst et al<sup>87</sup> carried out emf measurements across growing  $ZrO_2$  films at  $700^\circ C$  and suggested on this basis that electron transport is rate controlling.

(2) The interpretation of activation energies will have more meaning if variation of oxidation constants with oxygen pressure is also observed. For example, if activation energy of a linear law is obtained and it is thought that phase boundary with adsorption equilibria is rate determining, one may then expect that at a constant temperature a continuous decrease of  $Q$  with increasing oxygen pressure will be observed according to the model produced by Ehrlich<sup>74</sup>. In case of parabolic rate law, one should similarly expect a constant  $Q$  independent of pressure for n-type of oxide as predicted by Wagner mechanism.

The literature shows that activation energies have often not been investigated as a function of pressure. Such work is highly commendable.

(3) The real cause that leads to breakaway oxidation for Zr is not known. As proposed by Cox<sup>82</sup>, it may occur due to preferential oxidation at the grain boundaries which produces differential stresses resulting in crack formation.

If Cox's hypothesis is true, oxidation of single crystals of Zr can help reveal some of the facts. The breakaway

should not occur in such case. Such work has not been done. The single crystals to be employed in such work may be produced by  $\alpha$ - $\beta$  thermal cycling (for example see Higgins and Soo<sup>88</sup>) since the metal does not readily lend itself to the conventional 'strain anneal' and 'controlled solidification' techniques for the production of single crystals.

(4) Results of differential thermal analysis would have more meaning if oxidation states at strategic peak-temperatures are investigated. Literature does not show work done in this direction.

(5) Knowledge about structure and stability of Zr- and Nb-oxides is scanty. A range of oxides (~~single~~<sup>simple</sup> and complex) of Zr and Nb may form. ASTM cards, (used for oxidized identification), and for that matter past literature, furnish very little knowledge about these oxides. Thus there is need to investigate individual oxides of Zr and Nb (Nb in particular, oxides of which are thought to be plenty but few are known) and the system Zr oxide - Nb oxide. Individual nitrides as well as oxynitrides of these metals should also be investigated thoroughly.

Investigations of interactions among oxides will help understand many processes occurring during reaction of the alloy. It may explain what essentially causes difference in the observed kinetics for the specimens subjected to different oxidizing media. It would then shed doubts and confusions created heretofore as a result of many immature reasonings

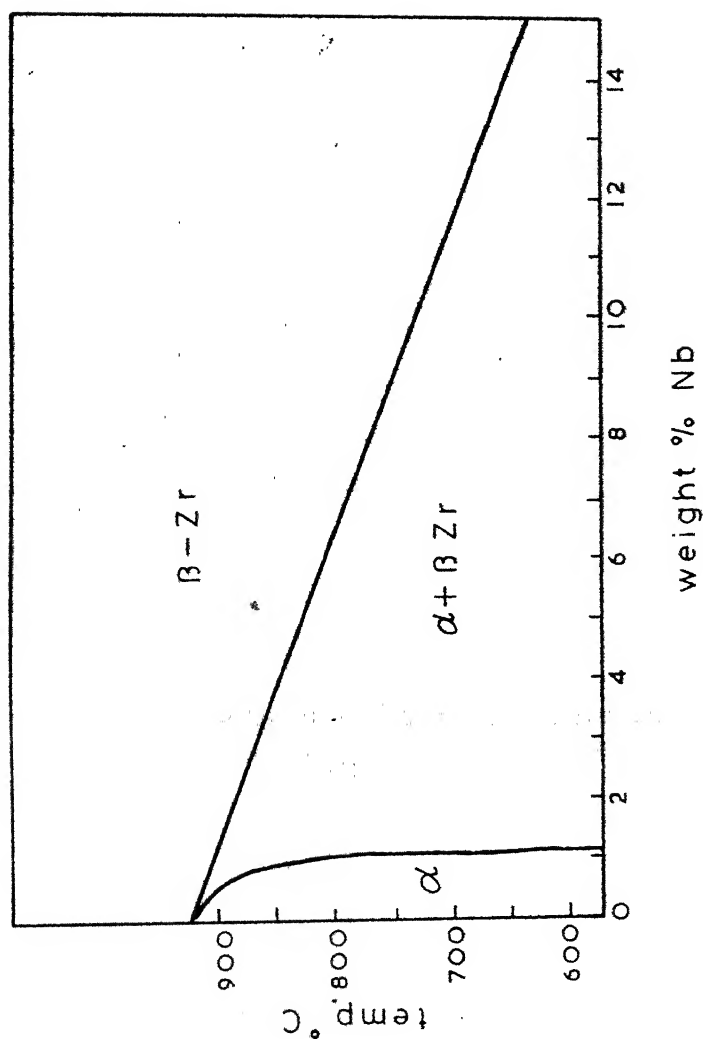
employed to explain the nature of the kinetics.

(6) Following two observations sought from the literature suggest that there is need to employ Electron Microscope in future investigations to settle many conflicts.

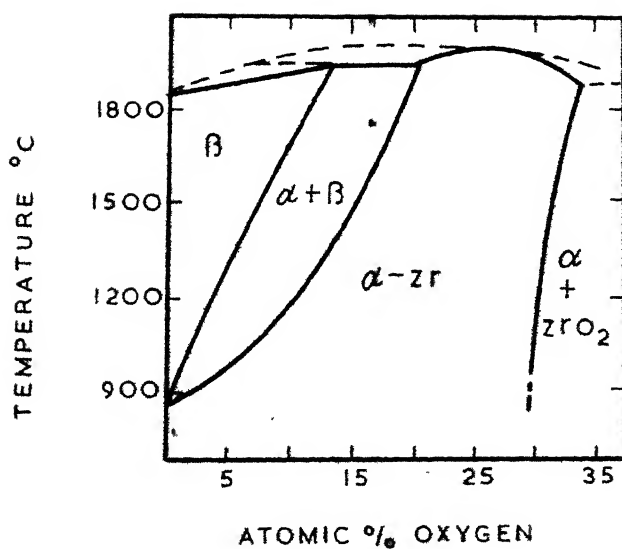
(a) Cox<sup>83</sup> recently attributed small pores (10-50 Å size) to be possibly responsible for the breakaway observed in the kinetics of pure Zr. He proposed that small pores are possibly formed as a result of some recrystallisation process. Electron microscope may thus be employed to reveal small pores of such size as mentioned. Also a knowledge of recrystallisation of the oxide is needed to establish the validity or the otherwise of the proposal made by Cox.

(b) In an electron microscope study of zirconium oxidation in air at 250 to 450°C, Douglass and van Landuyt<sup>20</sup> showed that the thin zirconia films as viewed by transmission microscopy were extremely heterogeneous despite the fact that the films showed uniform interference colours and exhibited smooth surfaces by the replication techniques. On this basis these authors questioned the usefulness of expressing the kinetic measurements in terms of particular rate equations.

## APPENDIX A



COMPOSITION OF  $\alpha$  AND  $\beta$  PHASES IN A Zr-2.5 WT % Nb  
ALLOY HOMOGENIZED IN THE RANGE 600-850 °C (After  
Bethune & Williams, J. Nucl. Mat., 29, 129 (1969))



### ZIRCONIUM-OXYGEN PHASE DIAGRAM

(After Gebhardt, Seghezzi and Diirrschnabel,  
J. Nucl. Mat., 4, 255 (1961))



## APPENDIX B

### ASTM Data for X-ray Analysis

Values of Interplanar Spacings (d) for the Three Strongest  
lines in the Powder Patterns

Materials	Ref. of the card	d(Å)	Rela- tive inten- sity (I/I <sub>1</sub> )	Remarks
$\alpha$ -Zirconium	5-0665	2.798	33	structure: hexagonal rel. intensity: diffracto- meter value is given Consists of 22 lower intensity lines upto d = 0.8201
		2.573	32	
		2.459	100	
Niobium	16-1	2.33	100	structure: cubic consists of 7 lower intensity lines upto d = 0.74
		1.649	20	
		1.348	20	
ZrO <sub>2</sub> (Baddeleyite)	13-307	3.157	100	structure: monoclinic rel. intensity: diffracto- meter value is given consists of 70 lower intensity lines upto d = 0.8852
		2.834	65	
		2.617	20	
Nb <sub>2</sub> O <sub>5</sub>	5-0352	3.931	100	rel. intensity: the values are obtained from visual estimate consists of 23 lower intensity lines upto d = 0.999
		3.140	100	
		2.447	70	
NbO	15-535	2.095	100	structure: cubic rel. intensity values: visual estimate consists of 22 lower intensity lines upto d = 0.7817
		1.484	100	
		1.267	100	

## Table of Appendix B contd...

NbO <sub>2</sub>	9-235	3.42	100	structure: tetragonal rel.intensity values: visual estimate consists of 17 lower intensity lines upto d = 1.754
		2.54	80	
		1.754	80	
Nb <sub>2</sub> N	12-437	1.807	90	structure: hexagonal rel.intensity values: visual estimate
		1.526	100	
		1.401	100	

---

## REFERENCES

1. Lustman, Bleiberg, Byron, Chirigos, Goodwin and Salvaggio, *Nucleonics*, 19, 58 (1961).
2. Robertson and Cox, *Nuclear News*, 7, 34 (1964).
3. Delgaard, AECL No. 993, Chalk River, Ontario (1960).
4. Cox, Davies and Johnston, AERE - R 3257, Harwell, Berkshire (1960).
5. Gulbransen and Andrew, *Trans. Amer. Inst. Min. (Metall.) Engrs.*, 185, 515 (1949).
6. Cubicciotti, J. *Amer. Chem. Soc.*, 72, 4138 (1950).
7. Fast, *Photo Prints* 13, 22 (1940).
8. Boer, Z. *Anorg. Chem.* 148, 345 (1925).
9. Hayes and Roberson, *Trans. Electrochem. Soc.*, 96, 142 (1949).
10. Treco, J. *Metals*, (1953).
11. Kass, *Corrosion*, 23, 374 (1967).
12. Gondi and Missiroli, *Nuovo Cimento*, B 48 (2), 223 (1967).
13. Hillner, J. *Electrochem. Soc.*, 114 (3), 237 (1967).
14. Belle and Mallet, J. *Electrochem. Soc.*, 101, 339 (1954).
15. Porte, Vogel and Fischer, J. *Electrochem. Soc.*, 107, 506 (1960).
16. Gulbransen and Andrew, *Trans. AIME*, 209, 394 (1957).
17. Charles, Barnartt and Gulbransen, *Trans. AIME*, 212, 101 (1958).
18. Wallwork, Smeltzer and Rosa, *Acta Met.*, 12, 409 (1964).
19. Pemsler, J. *Nucl. Mat.*, 7, 16 (1962).
20. Douglass and van Landuyt, *Acta Met.*, 13, 1069 (1965).
21. Holmberg, et al., *Acta Chem. Scand.*, 15, 919 (1961).

22. Gebhardt, Seghezzi and Diirrschnabel, J. Nucl. Mat., 4, 255 (1961).
23. Domagla and Pherson, Trans. Am. Inst. min. (metall.) Engrs, 209, 238 (1954).
24. Pemsler, J. Electrochem. Soc., 111, 381 (1964).
25. Westerman, J. Electrochem. Soc., 111, 140 (1964).
26. Hickman and Gulbransen, Analyt. Chem., 20, 158 (1948).
27. Lynch, Vahldiek and Robinson, J. Am. Ceram. Soc., 44 (1961).
28. Wallwork and Jenkins, J. Electrochem. Soc., 106, 10 (1959).
29. Phalnikar and Baldwin, Proc. Amer. Soc. Test. Mat., 51, 1038 (1951).
30. Guldner and Wuten, Trans. Electrochem. Soc., 93, 223 (1948).
31. Hukagawa and Nambo, E.T.J., Tokyo, 5, 27 (1941).
32. Drawinieks, J. Amer. Chem. Soc., 72, 3568 (1950).
33. Kendall, Hanford Atomic Products Operation, Wash., Contract No. W-31-109-Eng. -52 (Sept. 1955).
34. Someno, Shinku, 3, 55 (1960).
35. Bridges and Fassel, J. Electrochem. Soc., 103, 326 (1956).
36. Begley, U.S. Air Force Tech. Rep., WADC-TR-57-344 (1957).
37. Hurlen, Kjellesdal, Markali, Norman, Central Inst. Ind. Res. Norway, Tech. Note No. 1 (1959).
38. Brauer, Z., znorg. allegm. chemie, 248, 1 (1941).
39. Hurlen, Madrid Inst. del hierro y del acero, 13, 714 (1960).
40. Sisco, 'Columbium and Tantalum', Wiley Publications (1963).
41. Schonberg, Acta Chem. Scand., 8, 208 (1954).
42. Guard, Savage, Swarthout, Trans. AIME, 239, 643 (1967).
43. Albrecht and Goode, Battelle Memorial Inst. Publ. BML-1360 (1959).
44. Inouye, in 'Proceedings' of Regional Conf. on Reactive Metals, AIME (1956).

46. Klopp, Battelle Memorial Inst., DIME Rept. 123 (1960).
47. Cox, Chadd, Short., U.K., At. En. AERE-R 4134 (C.A. 1963).
48. Dalgaard, At. En. Can. Ltd., AECL - 1513 (1962).
49. Bethune and Williams, J. Nucl. Mat., 29(1), 129 (1969).
50. Chaturvedi and Tangri, Trans. AIME, 245, 259 (1969).
51. Guerlet and Lehr, J. Nucl. Mat., 28, 165 (1968).
52. Bryant, J. Less Comm. Metals, 4(1), 62 (1962).
53. Fairlin et al., Vestn. Mosk. Univ., Khim., 23(5), 44 (1968).
54. Prokoshkin et al. (CA 1963, 1967).
55. Greenbaw and Harper, Electrochem. Tech., 4(3-4), 142 (1966).
56. Harrison et al., US At. En. (1965).
57. Robert and Goldberg - Trans. Met. Soc. AIME, 236(11), 1619 (1966).
58. Zmeskal et al., US At. En. ORO - 204 (1959).
59. Porte, Schnitzlein, Vogel and Fischer, J. Electrochem. Soc., 107, 506 (1960).
60. Hiltz, C.A. 1959.
61. Amsel et al., J. Nucl. Mat., 29(2), 144 (1969).
62. Argent and Phelps, Less - Common Metals, 2, 181 (1960).
63. Almore, Gregg and Jepson, Electrochem. Soc., 107, 495 (1960).
64. Dawson et al., Electrochem. Tech., 4 (3-4), 137 (1966).
65. Heindlhoffer and Larsen, Trans. Amer. Soc. Steel Treat., 21, 865 (1933).
66. Chirigos and Thomas D.E., TIB - 5084 (1952).
67. Douglass, IAEA Conf. on the Corrosion of Reactor Materials, Salzburg (1962).
68. Vest et al., J. Amer. Ceram. Soc., 47, 635 (1964).
69. Wanklyn, quoted by Evans in 'The Corrosion of Oxidation of Metals', Edward Arnold, London, p. 30 (1960).

70. Felten, J. Less Comm. Metals, 17, 199 (1969).
71. Mackay, Trans. AIME, 227, 1184 (1963).
72. Hussey and Smeltzer, J. Electrochem. Soc., 111, 564 (1964).
73. Hurlen, J. Inst. Metals, 89, 273 (1960-61).
74. Ehrlich, Phys. Chem. Solids, 1, 3 (1956).
75. Saur et al., Metall., 18, 704 (1964).
76. Quarrel, 'Niobium, Tantalum, Molybdenum and Tungsten' Elsevier Publications (1961).
77. Brauer, Rept. of a Conf., Univ. of Sheffield (Sept. 1960).
78. Lustman and Kerz, 'Metallurgy of Zirconium' (1955).
79. Brauer and Muler, XVI Cong. Int. Chimie Pure et Appl., Paris (1957).
80. Kofstad and Espevik, J. Electrochem. Soc., 112, 153 (1965).
81. Mayo, Shepherd and Thomas, Less - Common Metals, 2, 223 (1960).
82. Cox, Prog. Nucl. En., Ser. IV, 4, 166 (1961).
83. Cox, J. Nucl. Mat., 29, 50 (1969).
84. Schwartz et al. in ref. 78.
85. Kofstad, 'High Temp. Oxidn. of Metals', Wiley Publications (1966).
86. Cox and Johnston, Trans. AIME, 227, 36 (1963).
87. Bradhurst, Draley and Drunen, J. Electrochem. Soc., 112, 1171 (1965).
88. Higgins and Soo, J. Nucl. Mat., 22, 285 (1967).